© 2018. Published by The Company of Biologists Ltd | Journal of Cell Science (2018) 131, jcs206326. doi:10.1242/jcs.206326

RESEARCH ARTICLE

# Prolines in the α-helix confer the structural flexibility and functional integrity of importin-β

**Masahiro Kumeta, Hide A. Konishi, Wanzhen Zhang, Sayuri Sakagami and Shige H. Yoshimura***

## ABSTRACT

The karyopherin family of nuclear transport receptors is composed of a long array of amphiphilic α-helices and undergoes flexible conformational changes to pass through the hydrophobic crowding barrier of the nuclear pore. Here, we focused on the characteristic enrichment of prolines in the middle of the outer α-helices of importin-β. When these prolines were substituted with alanine, nuclear transport activity was reduced drastically *in vivo* and *in vitro*, and caused a severe defect in mitotic progression. These mutations did not alter the overall folding of the helical repeat or affect its interaction with cargo or the regulatory factor Ran. However, *in vitro* and *in silico* analyses revealed that the mutant lost structural flexibility and could not undergo rapid conformational changes when transferring from a hydrophilic to hydrophobic environment or vice versa. These findings reveal the essential roles of prolines in ensuring the structural flexibility and functional integrity of karyopherins.

**KEY WORDS: Importin, Karyopherin, Molecular flexibility, Molecular structure, Nuclear transport, Proline**

## INTRODUCTION

The nuclear pore complex (NPC) serves as the sole gateway for communication between the eukaryotic nucleus and cytoplasm by exchanging functional molecules. Both inbound and outbound molecules are controlled by the selective barrier formed in the central channel of the NPC. Molecules smaller than 40 kDa can pass through the NPC by passive diffusion, while larger proteins cannot pass through without the aid of transport mediators (for review, see Gorlich and Kutay, 1999). Karyopherin-β family proteins, which include importin-β (KPNB1) and CRM1 (exportin 1 or XPO1), form the largest group of transport mediators (20 members), and mediate the transport of distinct sets of cargo proteins (for reviews, see Mosammaparast and Pemberton, 2004; Pemberton and Paschal, 2005).

Many approaches using biochemistry, structural biology and bioinformatics have revealed the structure of the NPC and the properties of its components, called nucleoporins (Nups) (Cronshaw et al., 2002; Rout et al., 2000). The entire complex is composed of more than 30 different Nups, each of which exists as multiple copies. The central channel of the NPC comprises a number of unstructured (disordered) polypeptides carrying phenylalanine-glycine (FG) motifs (FG-Nups). FG-Nups are similar to other intrinsically disordered proteins in that they are rich in polar residues, such as serine and threonine, but distinct from them by the frequent presence of hydrophobic residues (phenylalanine). This unique amino acid composition enables FG-Nups to form a hydrogel, where hydrophobic interactions between the phenylalanine residues crosslink the disordered polypeptides into a gel-like matrix (Frey and Gorlich, 2006; Mohr et al., 2009). *In vivo*, a strong hydrophobic crowding barrier has been shown to form in the NPC, which is especially enriched at both peripheries of the pore (Konishi et al., 2017).

Karyopherin-β family proteins are designed to pass through the amphiphilic matrix of the NPC. The crystal structures of karyopherin-β family proteins exhibit significant similarities in their overall molecular shape, although their amino acid sequence similarities are very low (15–20% identity) (O'Reilly et al., 2011; Xu et al., 2010). Karyopherins are composed of 19–21 tandem repeats of HEAT (Huntingtin, elongation factor 3, protein phosphatase 2A and PI3-kinase TOR1) motifs, each containing two amphiphilic α-helices (A-helix and B-helix) connected by a short linker region (Chook and Blobel, 1999; Cingolani et al., 1999). This characteristic helical composition makes the entire karyopherin molecule amphiphilic, with the hydrophobic sides facing each other toward the inside of the molecule and the hydrophilic sides facing outward to the solvent (Fig. 1A). A long array of HEAT motifs (HEAT repeat) confers the entire molecule with structural flexibility, which plays important roles in its interactions with cargo proteins and RanGTP (Chook and Blobel, 2001; Conti et al., 2006; Forwood et al., 2010; Lee et al., 2000; Stewart, 2007).

The structural flexibility of karyopherins is also important for their passage through the pore. Previous structural analyses have revealed flexible structural changes of importin-β upon binding to its cargo (Cingolani et al., 2000) or under different solvent conditions (Yoshimura et al., 2014), and its conformational flexibility has been shown to be important for protein–protein interactions and nuclear translocation (Lee et al., 2000). Karyopherins bind firmly to FG-Nups through hydrophobic pockets between adjacent A-helices (Bayliss et al., 2000, 2002; Liu and Stewart, 2005; Otsuka et al., 2008). Substitution of these residues with polar or charged residues reduces the affinity of karyopherins for FG-Nups. Hydrophobic residues within the NPC induce conformational changes on karyopherins to expose more hydrophobic residues on the molecular surface, allowing the molecule to diffuse through the pore. The affinity of karyopherins to FG-Nups is also known to be modulated by the structural changes induced by binding to their cargos (Lott et al., 2010). These findings explain how karyopherins can overcome the hydrophobic NPC barrier. Other HEAT-motif-rich proteins (such as PPP2R1A and CAND1) can also pass though the NPC by themselves (Yoshimura et al., 2014), indicating that the HEAT motif is generally suitable for NPC passage.

One of the striking features that distinguishes the HEAT motif from other helical repeat motifs (such as TPR, Arm and Ankyrin) is

Graduate School of Biostudies, Kyoto University, Sakyo-ku, Kyoto, 606-8501, Japan.

*Author for correspondence (yoshimura@lif.kyoto-u.ac.jp)

M.K., 0000-0003-0050-5036; H.A.K., 0000-0001-9529-9321; S.H.Y., 0000-0001-6033-1301

**Received 15 May 2017; Accepted 6 November 2017**

Journal of Cell Science (2018) 131, jcs206326. doi:10.1242/jcs.206326

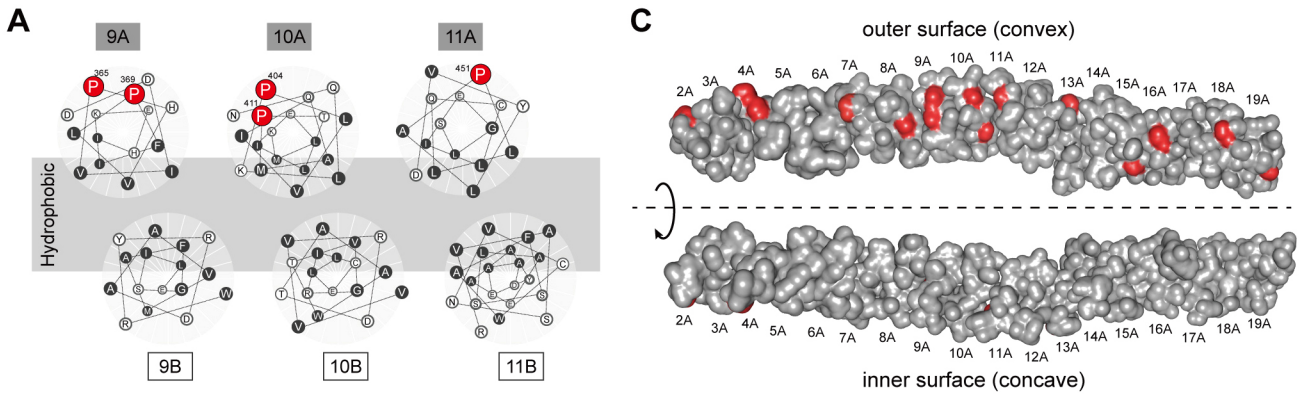


B

| HEAT # | A-helix (outer helix) | turn | B-helix (inner helix) | turn |
|---|---|---|---|---|
| 1 | melitilekt | vs**p**dr | leleaaqkfleraa | ve |
| 2 | nl**p**tflvelsrvlan | **p**gns | qvarvaaglqiknsl | tskd**p**dikaqyqqrwlaid |
| 3 | anarrevknyvlqt | lgtetyr**p** | ssasqcvagiacae | i**p**vs |
| 4 | qw**p**eli**p**qlvanvtn | **p**nst | ehmkestleaigyicqd | id**p** |
| 5 | eqlqdksneiltaiiq | gmrkee**p**s | nnvklaatnallnsle | ftkanfdk |
| 6 | eserhfimqvvceatqc | **p**d | trvrvaalqnlvkimsl | yyqym |
| 7 | etymg**p**alfaitieamk | sdi | devalqgiefwsnvcdeemdlaieaseaaeq | gr**pp**ehtskf |
| 8 | yakgalqylv**p**iltqtltk | qdendddddwn**p** | ckaagvclmllstc | ce |
| 9 | ddiv**p**hvl**p**fikehi | kn**p**d | wryrdaavmafgsile | g**p**e**p** |
| 10 | nqlk**p**lviqam**p**tlielmk | d**p**s | vvvrdttawtvgricell | **p**eaain |
| 11 | dvyla**p**llqcliegls | ae**p** | rvasnvcwafsslaeaayeaad | vaddqee**p**atycl |
| 12 | sssfelivqkllettd | r**p**dghqnn | lrssayeslmeivkn | sakd |
| 13 | cy**p**avqkttlvimerlqqvlq | meshiqst | sdriqfndlqsllcatlqnvlrk | vqh |
| 14 | qdalqisdvvmasllrmfqst | agsgg | vqedalmavstlvevl | gg |
| 15 | eflkymeafk**p**flgiglk | nyae | yqvclaavglvgdlcral | qs |
| 16 | nil**p**fcdevmqlllenl | gnenvhrs | vk**p**qilsvfgdialai | gg |
| 17 | efkkylevvlntlqqasqa | qvdksd | fdmvdylnelrescleaytgivqglk | gdqenvh**p** |
| 18 | dvmlvq**p**rvefilsfidhia | gdedht | dgvvacaagligdlcta | fg |
| 19 | kdvlklvear**p**mihelltegrr | skt | nkaktlatwatkelrklkn | qa |

**Fig. 1. Localization of proline residues in the convex surface of importin-β.** (A) Top view of HEAT motifs 9, 10 and 11. Importin-β contains 19 HEAT repeats, which are composed of two amphiphilic α-helices (A-helix and B-helix) facing each other by hydrophobic interactions. Red: proline; gray: hydrophobic amino acid. (B) Positions of the proline residues in mouse importin-β1. The amino acid sequence of mouse importin-β1 is shown by aligning the 19 HEAT repeats. Proline residues in the α-helices (A-helix and B-helix) are indicated by bold and highlighted in red. (C) Proline residues in the A-helices face toward the solvent. Surface representation of mouse importin-β based on its crystal structure (PDB: 1ukl). Only the A-helices are presented here (loops and B-helices are removed). All helices are aligned so they fit the same plane. Proline residues are indicated in red.

the presence of conserved proline residues in the A-helix (Chook and Blobel, 1999; Yoshimura and Hirano, 2016). Since the Cα–N bond of a proline residue in a peptide is incorporated in the Y-ring, the ϕ and ψ angles of proline are not suitable for α-helix formation. As a result of this, proline is known as the least likely of the 20 amino acids to be present in an α-helix and is widely regarded as an α-helical 'breaker' (O'Neil and DeGrado, 1990; Piela et al., 1987). Indeed, several mutational substitutions of an α-helix amino acid into proline are related to disease, including an alanine-to-proline mutation in a coiled-coil domain of keratin-10 (A158P) found in epidermolytic hyperkeratosis (Yang et al., 1997). Although it is known that a proline residue can form a kink in an A-helix (Cingolani et al., 1999), its functional significance has not been fully addressed. In this report, we focused on the proline residues in HEAT motifs and investigated their structural and functional roles. In particular, we examined how proline residues confer structural flexibility upon importin-β and achieve its efficient translocation through the NPC.

## RESULTS

### Cellular defects caused by proline-to-alanine mutations of importin-β

Through a global search of proline residues within karyopherins and other HEAT-rich proteins, many proline residues were found in the A-helix (outer helices) and loop regions that connect the A- and B-helices. Importin-β1 contains 15 proline residues in the A-helices, 21 in the loops, and 1 in the B-helices based on its crystal structure (Fig. 1B). Almost all of the proline residues in the A-helices are located at the molecular surface (convex face) and are in contact with solvent (Fig. 1C, Movie 1).

A series of mouse importin-β1 mutants were constructed in which all 15 prolines in the A-helices were mutated to alanine (ΔPro-all), together with strains containing a subset of the mutations (ΔPro-I, ΔPro-II, ΔPro-III and ΔPro-IV) (Fig. 2A). These mutants were expressed in HeLa cells in an enhanced green fluorescent protein (EGFP)-fused form. Anti-EGFP western blotting was performed against whole cell lysates obtained at

Journal of Cell Science (2018) 131, jcs206326. doi:10.1242/jcs.206326

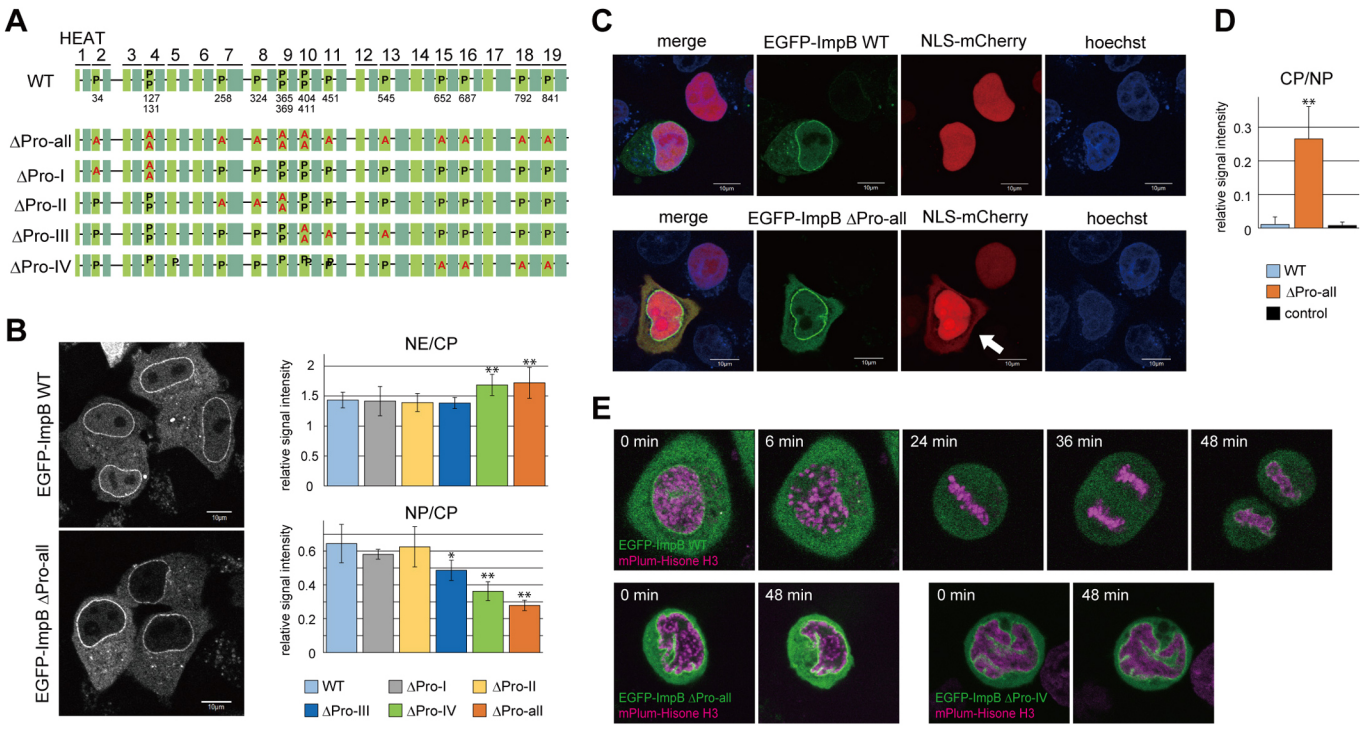


**Fig. 2. Functional defects of importin-β containing multiple proline-to-alanine mutations.** (A) Design of the proline mutants. Among the 15 prolines in the A-helices, all (ΔPro-all) or 3–4 neighboring ones (ΔPro-I, II, III and IV) were substituted with alanine (indicated by red). Light green: HEAT A-helix; dark green: B-helix; P: proline; A: alanine. (B) HeLa cells were transfected with plasmids to express EGFP–importin β1 (WT: wild-type and ΔPro mutants). The images for the EGFP signal of wild-type and ΔPro-all are shown on the left. Averaged signal intensities for the nuclear envelope, nucleoplasm (excluding nucleolar regions), and cytoplasm were quantified, and the ratios for the nuclear envelope to cytoplasm (NE/CP) and nucleoplasm to cytoplasm (NP/CP) were analyzed statistically for all the mutants. Error bars represent ±s.d. ($n$=10). Asterisks indicate statistically significant differences compared with the wild-type protein (*$P$<0.05, **$P$<0.01 using Student's $t$-test). (C) HeLa cells were transfected with plasmids to express EGFP–importin-β1 (wild-type and ΔPro-all) and NLS–mCherry. At 20 h after transfection, the cells were fixed, counterstained with Hoechst 33342, and observed by confocal microscopy. Cells expressing ΔPro-all showed a significant increase in the cytoplasmic population of NLS–mCherry (indicated by the arrow). (D) Statistical analysis of the cytoplasmic population of NLS–mCherry in HeLa cells expressing EGFP–importin β1 (wild-type and ΔPro-all). Error bars represent ±s.d. ($n$>5). Asterisks indicate statistically significant differences compared with the wild-type protein (**$P$<0.01). EGFP non-expressing cells were analyzed in the same way as a control. (E) Live HeLa cells expressing EGFP–importin-β1 (wild-type, ΔPro-all and ΔPro-IV) and mPlum–histone-H3 were observed under a microscope. Collapse and reconstruction of the nuclear envelope were observed clearly along with mitotic progression in wild-type importin-β1-expressing cells (top panels). The cells expressing ΔPro-all and ΔPro-IV showed severe defects in mitotic progression (bottom panels).

24 h post-transfection to confirm expression of the full-length molecules. A single band at the expected molecular mass (~120 kDa) was obtained in all mutants, suggesting similar stability among them (Fig. S1A). The subcellular localization of the wild-type and mutant proteins was observed by confocal laser-scanning microscopy (Fig. 2B and Fig. S1B). Cells with similar EGFP expression levels were selected by quantifying cellular fluorescent intensity to analyze the subcellular localization of the mutants (Fig. S1C). Averaged signal intensities at the nuclear envelope, nucleoplasm and cytoplasm were quantified and their ratios were analyzed statistically for all of the mutants. The results clearly showed that ΔPro-IV and ΔPro-all accumulated more in the nuclear envelope and less in the nucleoplasm compared with the wild-type protein (Fig. 2B). ΔPro-III also showed significantly reduced nuclear accumulation than the wild-type protein, suggesting the importance of C-terminal prolines in the nuclear transport of importin-β. When EGFP–ΔPro-all was expressed in HeLa cells, significant deformation of the shape of the nucleus was observed, which accompanied the apparent increase in the cytoplasmic population of the NLS-cargo protein (Fig. 2C,D). This suggests a functional defect of the ΔPro-all mutant that causes an aberration in the importin-β-dependent nuclear transport pathway. This mutant also caused severe defects in mitotic progression. Time-lapse observations revealed that cells expressing ΔPro-all were arrested at the beginning of prophase, showing a defect in breakdown of the nuclear envelope (Fig. 2E, Movies 2 and 3). Cells expressing EGFP–ΔPro-IV exhibited similar mitotic defects to those expressing ΔPro-all ($n$=11 for ΔPro-IV and $n$=11 for ΔPro-all), and the aberrant cells eventually died after approximately 3 h arrest at the beginning of mitosis (Fig. S2). These results demonstrated a dominant-negative effect of the ΔPro-IV and ΔPro-all mutants *in vivo* that may be the result of a defect in their nuclear transport ability.

### Proline mutations in importin-β affect its transport through the NPC

The passage of the mutants through the NPC was examined *in vivo* by fluorescence recovery after photobleaching (FRAP) analysis. After bleaching the fluorescence signal in the nucleus, including the nuclear envelope, signal recovery was monitored by time-lapse imaging (Fig. 3A). Fluorescence recovery was analyzed separately for the nuclear envelope and nucleoplasm (Fig. 3B,C). Compared with the fast recovery of the wild-type protein for both the nuclear envelope and nucleoplasm, the accumulation of the ΔPro-all mutant was significantly slower for both compartments. Final fluorescence recovery ($I_{final}$) and association rate constant ($k_{on}$) for

Journal of Cell Science (2018) 131, jcs206326. doi:10.1242/jcs.206326

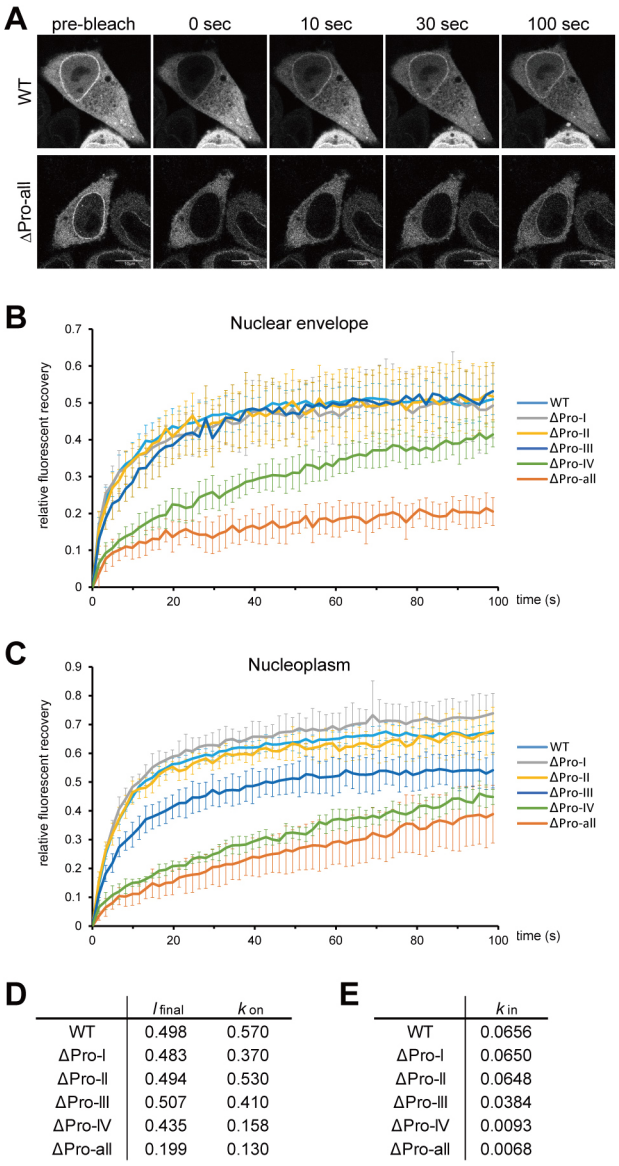


D

| | $I_{final}$ | $k_{on}$ |
|---|---|---|
| WT | 0.498 | 0.570 |
| ΔPro-I | 0.483 | 0.370 |
| ΔPro-II | 0.494 | 0.530 |
| ΔPro-III | 0.507 | 0.410 |
| ΔPro-IV | 0.435 | 0.158 |
| ΔPro-all | 0.199 | 0.130 |

E

| | $k_{in}$ |
|---|---|
| WT | 0.0656 |
| ΔPro-I | 0.0650 |
| ΔPro-II | 0.0648 |
| ΔPro-III | 0.0384 |
| ΔPro-IV | 0.0093 |
| ΔPro-all | 0.0068 |

**Fig. 3. FRAP analysis reveals slower nuclear shuttling of the mutants.** (A) HeLa cells expressing EGFP-fused importin-β were subjected to FRAP analysis. Captured images at the indicate time after bleaching. (B) Quantification of fluorescence recovery for wild-type and proline-mutated importin-β at the nuclear envelope. The signal intensity of the nuclear envelope region relative to pre-bleach signals was analyzed statistically (bars: ±s.d., *n*=6). (C) Fluorescence recovery at the nucleoplasm was analyzed in the same way as in B. (D) Curve fitting analysis using an exponential association model was performed for the recovery observed at the nuclear envelope shown in B. Estimated final fluorescence intensity ($I_{final}$) and association constant ($k_{on}$) are represented. (E) Recovery at the nucleoplasm shown in C was used to estimate the import rate constant ($k_{in}$) by curve fitting.

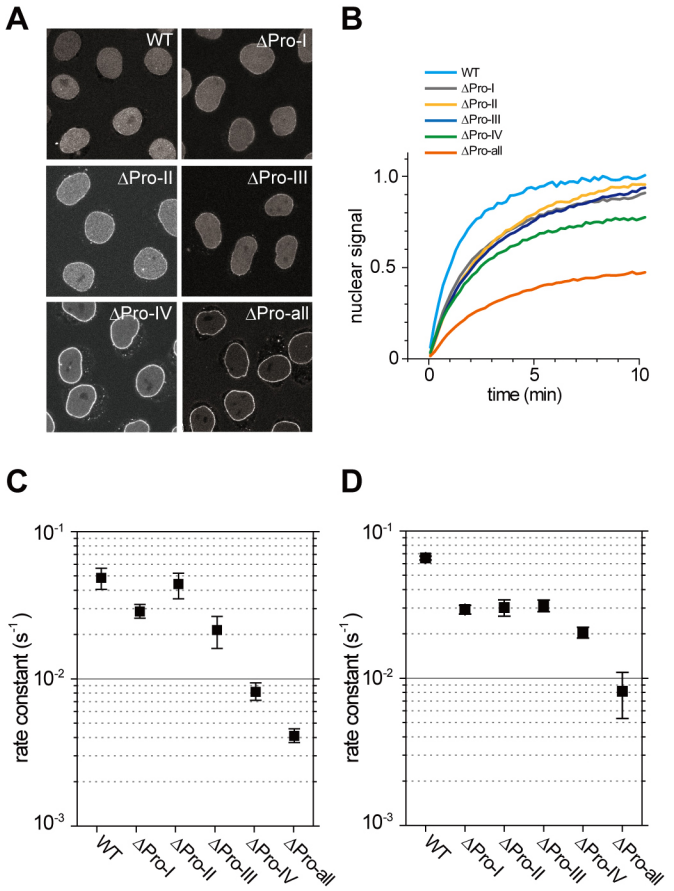


**Fig. 4. Proline-to-alanine mutants show lower transport rates through the NPC *in vitro*.** (A) Kinetic measurement of importin-β transport into the nucleus through the NPC. Purified EGFP-fused importin-β (wild type and mutants) was added to digitonin-treated HeLa cells, and time-lapse observations under a fluorescence microscope were performed. Snapshot images at 3 min after adding importin-β are shown. (B) Nuclear accumulation of fluorescence signal accumulation quantified and analyzed statistically. (C) The influx rate constant ($k_{in}$) for free importin-β was obtained by curve fitting analysis (bars: ±s.d., *n*>10). (D) Influx rate constants for the importin-β–IBB complex (bars: ±s.d., *n*>10).

the nuclear envelope were estimated by exponential association fitting (Sprague et al., 2006) (Fig. S3). Although $I_{final}$ values may not be directly comparable owing to the different amounts of bleached populations between the analyses (Fig. 2B), the results indicate distinctively smaller recovery and attenuated association of the ΔPro-all mutant to the nuclear envelope (Fig. 3D). Nuclear import kinetics were also analyzed by fitting fluorescent recovery at the nucleoplasm as described previously (Kumeta et al., 2012). The import rate ($k_{in}$) for ΔPro-all was one order of magnitude smaller than that of the wild-type protein, clearly showing a defect in its translocation through the NPC (Fig. 3E). Among the partial mutants, ΔPro-III showed significantly slower nucleoplasmic recovery and ΔPro-IV exhibited significantly reduced recovery for both the nuclear envelope and nucleoplasm compared with the wild-type protein, suggesting the importance of the C-terminal prolines.

The detailed kinetic properties of the mutants were analyzed further using an *in vitro* transport assay. EGFP-fused mutant importin-β, as well as the wild-type protein, were expressed in bacteria, purified by affinity chromatography and incubated with digitonin-treated HeLa cells. Time-lapse observations showed that all mutants tended to accumulate in the nuclear envelope, resulting in slower nuclear accumulation (Fig. 4A,B). In good agreement with the FRAP analysis, the influx rate constant of the ΔPro-all mutant was one order of magnitude smaller than that of the wild-type protein (Fig. 4C). The same experiment was performed with cargo-loaded importin-β by using the importin-β binding domain (IBB) of importin-α. All of the IBB-bound mutants exhibited smaller influx rate constants than those measured for the wild-type protein (Fig. 4D).

Journal of Cell Science (2018) 131, jcs206326. doi:10.1242/jcs.206326

### Effect of proline-to-alanine substitutions on the molecular interactions of importin-β

A gel filtration assay was performed using purified wild-type and ΔPro-all importin-β to investigate their oligomeric status. Although the elution peak was slightly different for wild-type and ΔPro-all importin-β, both showed a single peak, indicating that they both exist as monomers (Fig. 5A). The role of proline in the interaction of importin-β with RanGTP and cargo proteins was then examined using a pull-down assay. All of the single mutants and multiple mutants exhibited similar affinity to RanGTP (Fig. 5B) and to the IBB (Fig. 5C) in the μM range, which is similar to that in the cytoplasm. These results indicate that proline-to-alanine mutations in the A-helix do not affect the interaction of importin-β with cargo or RanGTP. This is reasonable because the import cargo and Ran mainly interact with the concave surface (B-helix) of importin-β, whereas the proline residues are located at the convex surface (A-helix). The interaction of importin-β with FG-Nups [full-length Nup54, FG-rich regions of Nup62 (amino acid residues 1–178) and Nup153 (amino acid residues 896–1475)] was also analyzed using a pull-down assay. These nucleoporins play important roles in transport kinetics and have high affinity to their import cargos (Ben-Efraim and Gerace, 2001). Relative quantification of the amount of bound protein clearly showed enhanced binding of the ΔPro-all and ΔPro-IV mutants with Nup62 and Nup153, but not with Nup54 (Fig. 5D). Considering that the interaction of karyopherins and FG-Nups is hydrophobic in nature, these mutants may assume different molecular conformations that are more suitable for interacting with Nups than the wild-type protein.

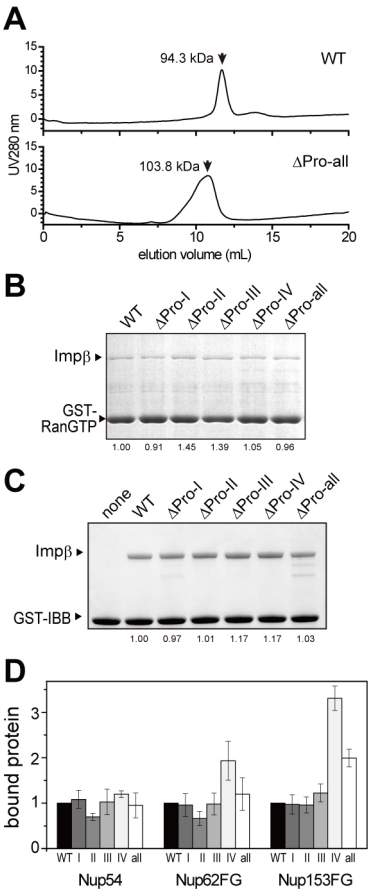


**Fig. 5. Molecular properties of wild-type and mutant importin-β.** (A) The elution profiles of wild-type (top graph) and ΔPro-all mutant (bottom graph) importin-β by gel filtration. On the basis of the elution profiles of the molecular markers (not shown here), the molecular masses of wild-type and mutant importin-β were estimated to be 94.3 and 103.8 kDa, respectively. (B) Binding assay of importin-β to RanGTP. GST–RanGTP was immobilized on beads and wild-type and mutated importin-β were added. An SDS-PAGE gel stained with Coomassie Brilliant Blue (CBB) is shown. The bands corresponding to importin-β and Ran are indicated by arrowheads. The relative amounts of importin-β bound to Ran-GTP were quantified and are presented below the gel. (C) Binding assay of importin-β to the IBB. GST–IBB was used for this assay. An SDS-PAGE gel stained with CBB is shown. The bands corresponding to importin-β and the IBB are indicated by arrowheads. The relative amounts of importin-β bound to IBB were quantified and are presented below the gel. (D) Results of the binding assay with Nups. Full-length Nup54, FG-repeat regions of Nup62 (amino acid residues 1–178) and Nup153 (896–1475) were used for the assay. The relative amounts of importin-β bound to the Nups immobilized on beads were quantified and are shown in the graph (bars: ±s.d., $n$=3).

### Loss of proline causes a loss of helical flexibility

To understand further the effect of the mutations on structural stability, molecular analyses were performed using recombinant proteins purified from bacteria. When analyzed by circular dichroism (CD) spectra measurements, all of the ΔPro mutants and wild-type importin-β exhibited a typical α-helix-rich spectrum with two characteristic negative peaks at 208 and 222 nm (Fig. S4). Proline-to-alanine substitutions slightly enhanced this signal, but did not significantly affect the spectra peaks, suggesting that the ΔPro mutants retain similar α-helical content to that seen in the wild-type protein. The tertiary structure of importin-β was evaluated by the fluorescence spectrum of tryptophan residues. Folding free energy ($\Delta G_0$) was estimated from a shift of peak center wavelength with increasing concentrations of urea (0–9 M) (Fig. S5A). When compared with a globular protein [bovine serum albumin (BSA)], importin-β showed smaller $\Delta G_0$ and cooperativity, indicating that helical repeat proteins have a weaker hydrophobic core than globular proteins (Fig. 6A). The addition of amphiphilic molecules, such as trifluoroethanol (TFE), which have been demonstrated to mimic the hydrophobic environment of the NPC (Yoshimura et al., 2014), altered the peak center shift and reduced the folding energy of importin-β (Fig. 6A,B, and Fig. S5B). These results imply that the hydrophobic core of importin-β, which consists of amphiphilic α-helices of HEAT repeats, is weakened in the NPC.

The effect of the proline mutations on the folding free energy of importin-β was then examined. Apparent folding free energy ($\Delta G_0$) was estimated by observing the irreversible unfolding curve of the purified proteins. A comparison of $\Delta G_0$ between the wild-type and ΔPro mutants revealed that the ΔPro-IV and ΔPro-All mutants showed significantly larger $\Delta G_0$ values than the wild-type protein, whereas the other mutants showed comparable or even smaller values (Fig. 6A and Fig. S6). These results indicate that mutations in the C-terminal HEAT motifs reduce molecular flexibility, which resulted in the aberration of nuclear transport ability (Figs 2 and 3).

The role of proline residues in the structural flexibility of importin-β was also analyzed by measuring the hydrophobicity of the protein surface. The hydrophobic fluorescent probe bis-ANS binds to the hydrophobic surface of proteins and emits strong fluorescence. When using a low concentration of the probe (0.1–10 μM), the fluorescent intensity of the ΔPro-all mutant was slightly higher than that of wild-type importin-β (Fig. 6C). This is consistent with the results of the binding assays, indicating that the molecular surface of the mutant is slightly more hydrophobic than that of the wild-type protein in an aqueous solution. When the concentration of bis-ANS was increased, the wild-type protein showed a drastic increase in fluorescence intensity whereas ΔPro-all exhibited a considerably smaller change. A comparison of the fluorescence

Journal of Cell Science (2018) 131, jcs206326. doi:10.1242/jcs.206326

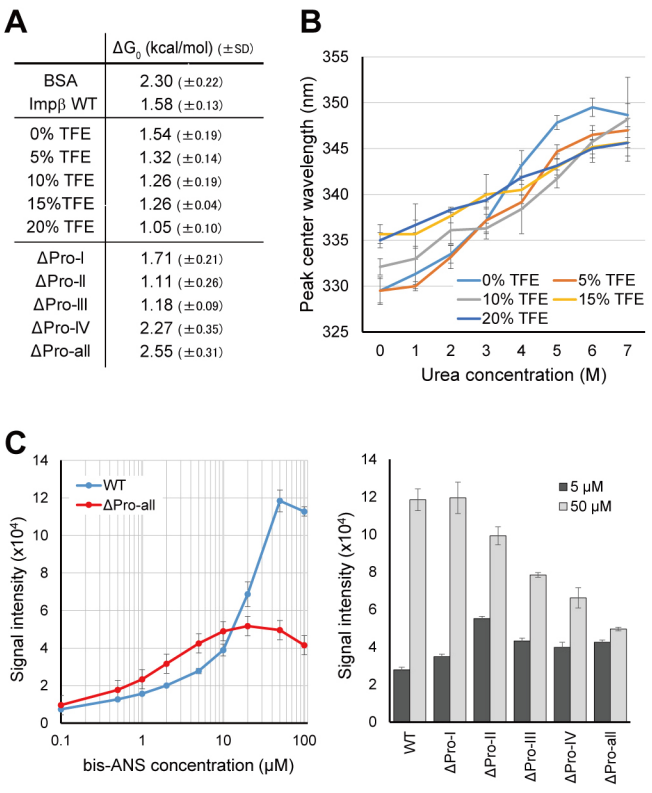


**Fig. 6. Structural analyses of wild-type and mutant importin-β.** (A) Folding free energy ($\Delta G_0$) of importin-β calculated by a urea-induced denaturation assay. Purified wild-type and mutant importin-β were prepared at a concentration of 37 μg/ml, tryptophan fluorescence was measured in the presence of 0–9 M urea, and $\Delta G_0$ was calculated by analyzing the shift in peak center wavelength. The estimated values for wild-type and mutant importin-β are presented, as well as for bovine serum albumin (BSA) as a representative standard globular protein (top panel). The $\Delta G_0$ values in different hydrophobic environments were calculated by the same urea denaturation assay in the presence of 0–20% TFE for wild-type importin-β (bottom panel). The results are the average of more than three independent measurements. The tryptophan fluorescent spectra are shown in Figs S5 and S6. (B) Peak center shift of wild-type importin-β under 0–7 M urea in the presence of 0–20% TFE. The spectra are shown in Fig. S5. (C) Surface hydrophobicity measurement of importin-β using the hydrophobic fluorescent probe bis-ANS. The concentration of bis-ANS was titrated from 0.1 to 100 μM, and averaged fluorescence intensities are plotted (left, bars: ±s.d., $n$>3). Fluorescence intensities at 5 and 50 μM are shown in the bar graph (right).

intensity at 50 μM bis-ANS with that at 5 μM clearly showed differences between the wild-type and mutant proteins (Fig. 6C). It is reasonable to conclude that wild-type importin-β underwent a structural change in response to the hydrophobic environment to expose more of its hydrophobic area to the molecular surface. The ΔPro-all mutant clearly lacks this molecular flexibility and was unable to adapt to the hydrophobic environment.

### Molecular dynamics simulation reveals the role of proline residues in the flexibility of the α-helix

Molecular dynamics simulation was performed to understand the molecular mechanism of structural flexibility conferred by proline residues. The crystal structure of importin-β [Protein data bank (PDB) ID: 1ukl] was used as the initial structure for the simulation. The proline mutant (ΔPro-all) was constructed by replacing the proline residues in the A-helices by alanine in the PDB data. The structures of wild-type and ΔPro-all mutant importin-β in water did not show significant differences in their overall molecular shape (Fig. 7A,B). In good agreement with the results from the CD spectra and bis-ANS binding assays, detailed structural analyses revealed that the structure of individual α-helices was not significantly affected by the loss of proline residues; helix length, helix–helix distance and the kink angle of the helix were all similar between wild-type and ΔPro-all mutant importin-β (Fig. 7A,B, and Fig. S7).

The simulation was then performed in a 50% water:50% TFE mixture to reveal structural flexibility in a hydrophobic environment. We have demonstrated previously that a water/TFE mixture mimics the environment within the NPC because of its amphiphilic property (Yoshimura et al., 2014). When wild-type and ΔPro-all mutant importin-β were transferred to the water/TFE mixture, they started to change conformation and ended up with a partly altered structure (Fig. 7C,D,G). As demonstrated in our previous study, wild-type importin-β started to unfold its helical repeat partially, especially at the C-terminal HEAT repeats (HEAT 15–18). Surprisingly, structural fluctuations of these helices were increased in the presence of TFE, even though TFE is known to stabilize α-helical structures. This suggests that the α-helices in the HEAT repeats are stabilized mainly by hydrophobic interactions between helices, and not by hydrogen bonds within the helices. The effect of TFE was smaller on the ΔPro-all mutant than on the wild-type protein. The change of root mean square deviation (RMSD), as well as the fluctuation of individual A-helices, was significantly smaller in the ΔPro-all mutant than in wild-type protein only in the water/TFE mixture (Fig. 7E–G). It is interesting to note that such differences were found not only in proline-containing helices (HEAT 15A and 16A) but also in helices lacking proline (HEAT 17A). This implies that not only intra-helix interactions but also inter-helix interactions play an important role in the stability of HEAT repeats.

The reversibility of the TFE-induced structural change was analyzed by transferring the molecules at certain time points of simulation (100 or 200 ns) from 50% water:50% TFE to 100% water. The wild-type protein reconverted rapidly to its original structure, whereas the ΔPro-all mutant barely changed status (Fig. 7H). These results demonstrated that the structural flexibility and reversibility of importin-β is maintained cooperatively by multiple prolines in the α-helices that are facing the solvent.

## DISCUSSION

### Effect of proline residues in α-helical repeats

The structural role of proline residues in the loop regions has been investigated in many proteins. They play a key role in the regulation of molecular conformation and function, as was revealed for the ion channel 5-hydroxytryptamine type-3, in which a proline residue in a loop region undergoes *cis–trans* isomerization and functions as an open–close switch (Lummis et al., 2005). Conversely, the structural and functional roles of prolines in helices have been studied less. Many examples of proline residues in α-helices were found in the protein structural database. Many of them formed a kink in the helix with fixed ϕ and ψ angles of −60° and +20° to +30°, respectively (Barlow and Thornton, 1988). These were mostly found in the transmembrane α-helices of channels and receptors, such as bacteriorhodopsin and transmembrane conductance regulator, to create a suitable channel space within a membrane (Henderson et al., 1990; Luecke et al., 1999; Mitsuoka et al., 1999; Wigley et al., 2002).

Prolines in α-helices are one of the unique characteristics of karyopherins and some other HEAT-repeat-containing proteins (Yoshimura and Hirano, 2016). Although these prolines locally break or kink each α-helix, the entire molecule retains a helical

Journal of Cell Science (2018) 131, jcs206326. doi:10.1242/jcs.206326

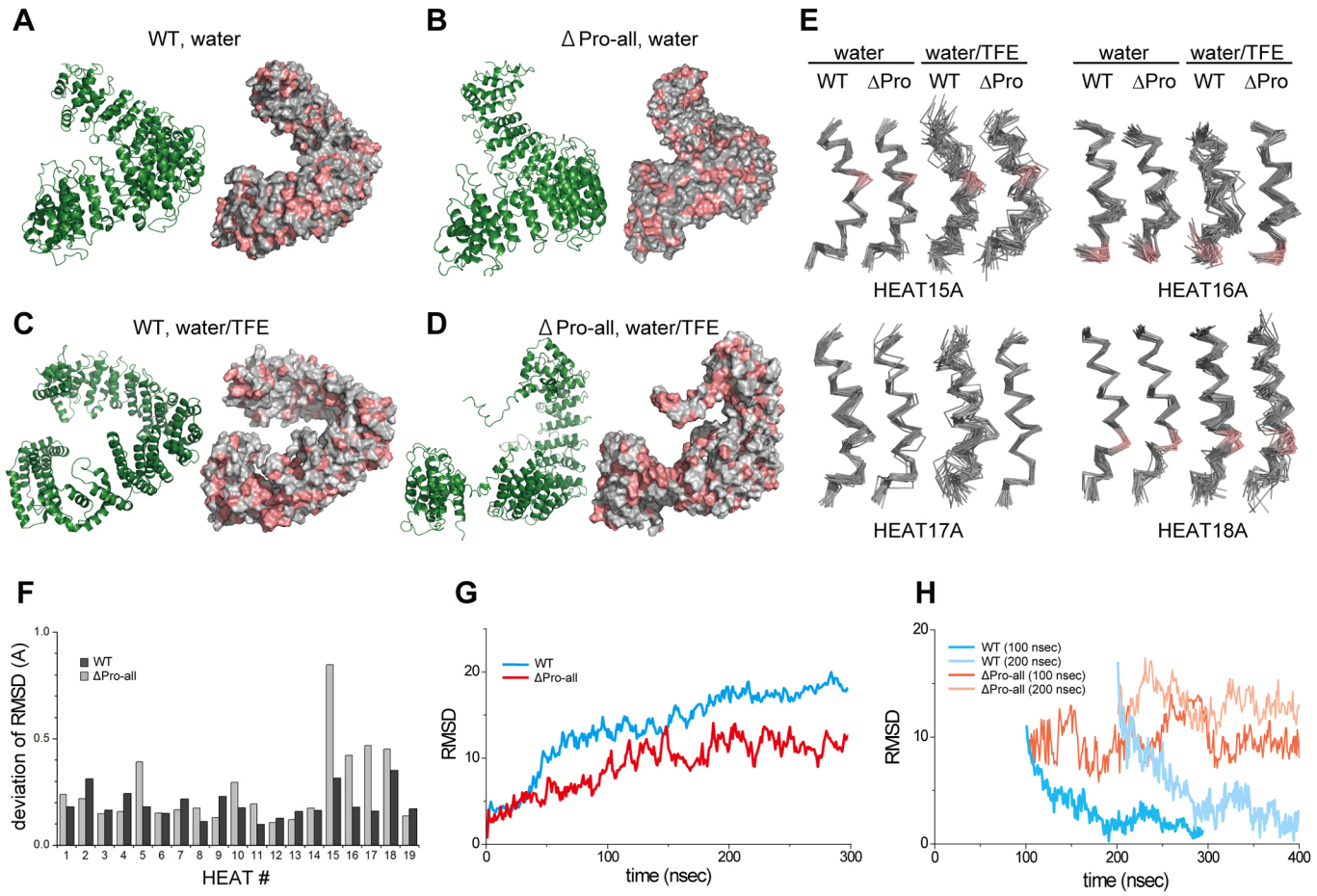


**Fig. 7. Molecular dynamics simulation reveals the essential role of prolines in the structural maintenance of importin-β.** (A–D) Molecular dynamics simulation of wild-type (A,C) and ΔPro-all mutant (B,D) importin-β in water (A,B) or a 50% water:50% TFE mixture (C,D). The structures at 200 ns are presented as a ribbon diagram (left) and surface plot (right). Hydrophobic residues are labeled in red in the surface plot. (E) Fluctuations of the A-helix. The main chain of the indicated A-helix is overlaid every 10 ns. The proline and substituted alanine residues are shown in red. (F) The fluctuations of the helices in 50% water:50% TFE were quantified by analyzing deviations of the RMSD for each helix. (G) The RMSD of entire wild-type and ΔPro-all importin-β molecules simulated in 50% water:50% TFE solvent (blue: wild-type, red: ΔPro-all mutant). (H) Structural changes induced by transferring molecules from 50% water:50% TFE to 100% water. From the trajectory shown in G, molecules at 100 or 200 ns were transferred into water and simulated further. The RMSDs for wild-type (blue: transferred at 100 ns, light blue: 200 ns) and ΔPro-all mutant (orange: 100 ns, light orange: 200 ns) are shown.

solenoid configuration when analyzed in water (Fig. 7A). This might be because the destabilizing effect of prolines is compensated by a stabilizing effect exerted by adjacent interacting α-helices in the helical repeat. Indeed, the substitution of proline to alanine largely affects the structure of isolated peptides, but not the entire molecule of importin-β (Fig. 7B). Analysis of the molecular trajectory showed no clear relation between proline residues and structural fluctuations of α-helices (Fig. 7E,F, and Fig. S7); proline-containing helices showed a similar level of fluctuation as proline-free helices in water. These results demonstrate that the destabilizing effect of prolines in each helix is compensated by interactions with adjacent helices in a long array of helices.

In contrast to the hydrophilic environments of the cytoplasm and nucleoplasm, the destabilizing effect of proline seems to be prominent in hydrophobic environments, such as the central channel of the NPC, in which a protein matrix made by FG-Nups prevents soluble proteins and other macromolecules from traveling through the pore. Phenylalanine residues and other hydrophobic groups interact with the outer helices of HEAT repeats and loosen helix–helix interactions. So far, several strong binding pockets for the FG motif have been identified in the cleft between two adjacent A-helices (Otsuka et al., 2008). In such a protein-rich environment, the destabilization effect of proline dominates the stabilizing effect from helix–helix interactions, and loosens the overall folding of the helical repeat, which further accelerates the interaction with FG-Nups. This conformational change is crucial for passing through the protein-rich environment of the NPC. Our results demonstrated that the ΔPro-all mutant was more stable and less flexible than the wild-type protein (Figs 6 and 7). It is reasonable to conclude that the substitution of proline to alanine deprives the α-helix of its destabilizing force, and prevents flexible conformational changes in an FG-rich protein crowding environment.

It should be noted that the effect of proline-to-alanine substitutions was more prominent in the C-terminal HEAT repeats than in the N-terminus. In comparison with the ΔPro-all mutant, the ΔPro-IV mutant exhibited similar subcellular localization (Fig. 2B) and FRAP at the nucleoplasm (Fig. 3C), but significantly faster FRAP at the nuclear envelope (Fig. 3B). Taken together with their similar folding stability (Fig. 6A), C-terminal HEAT repeats are likely to play a central role in maintenance of the flexibility of the entire molecule, which is important mainly in the release of importin-β into the nucleoplasm. In addition to the well-characterized N-terminal Nup-binding region around HEAT 5–7 (Bayliss et al., 1999; Chi and Adam, 1997; Kose et al., 1997), the

Journal of Cell Science (2018) 131, jcs206326. doi:10.1242/jcs.206326

C-terminal region corresponding to HEAT 14–16 was also shown to interact with Nups (Bednenko et al., 2003). Both the N- and C-terminal Nup-binding regions were shown to contribute to nuclear transport to a similar extent. Nups may have a preference for the N- or C-terminal binding sites of importin-β, as a C-terminal proline-to-alanine mutation affected interactions with only a subset of FG-Nups (Fig. 5D). As the effect of proline-to-alanine substitutions was observed not only in the proline-containing helices but also in the proline-free ones (Fig. 7E,F), it is reasonable to suggest that multiple prolines work cooperatively to ensure the global molecular structure of importin-β.

### Defects in nuclear transport and mitotic nuclear envelope breakdown in cells expressing ΔPro-all

It is reasonable to assume that the ΔPro-all mutant of importin-β possesses less association efficiency and far less dissociation efficiency to the NPC than that seen in the wild-type protein. This can explain its reduced localization to the nucleus *in vivo* (Fig. 2B), slower accumulation in the nucleoplasm and nuclear envelope *in vivo* (Fig. 3) and smaller influx rate *in vitro* (Fig. 4). Therefore, the mutant has a longer retention time at the pore, blocks the endogenous transport factors, and might lead to severe cellular defects. Our findings provide direct evidence of a structure–function correlation in the nuclear transport mechanism: loss of adaptive molecular flexibility leads to an aberration in nuclear transport.

Expression of the ΔPro-all mutant in HeLa cells caused a severe defect in mitotic progression; the cells were arrested at prophase with an aberration in breaking down the nuclear envelope (Fig. 2). Importin-β is known to play an important role in mitosis, especially in the mid-to-late stage to organize the spindle and reassemble a functional nuclear envelope. Importin-β generally plays negative roles in these steps through its interaction with Ran (reviewed by Harel and Forbes, 2004; Hetzer et al., 2002), by chelating spindle-organizing factors and Nups (Ciciarello et al., 2004; Harel et al., 2003; Nachury et al., 2001). In contrast, little is known about the role of importin-β in nuclear envelope breakdown. A study using an *in vitro* nuclear disassembly system with *Xenopus* egg extracts demonstrated that excess RanGTP as well as the IBB and BSA-NLS inhibited nuclear envelope breakdown (Muhlhausser and Kutay, 2007). This finding suggests a role for importin-β in sequestering nuclear envelope proteins such as lamins or other inner nuclear membrane proteins, leading to the rupture of the nuclear envelope during prophase. Since the ΔPro-all mutant had reduced cargo transport activity (Fig. 2), its overexpression could disturb the subcellular localization of factors needed for nuclear membrane breakdown.

Depletion of Nup153 was shown to lead to a severe cellular defect at the early stage of mitosis, which resulted in a characteristic multilobed nucleus (Mackay et al., 2009). Since the mitotic defect induced by overexpressing the ΔPro-all mutant was observed at a similar stage of mitosis, there may be functional crosstalk between importin-β and Nup153 to regulate the early stage of mitosis. Analysis of the binding proteins that differentially associate with wild-type and mutant proteins will clarify the responsible factor for the observed mitotic arrest, and will reveal novel mechanisms of how importin-β controls nuclear envelope breakdown.

### Evolutionary conservation of proline-containing α-helices

Karyopherin family proteins are found in a diverse range of eukaryotic species, and homologs of importin-β are found in most eukaryotes (O'Reilly et al., 2011). The amino acid sequences of importin-β1 from a variety of eukaryotic species were aligned against that of human importin-β1 to compare the number and position of proline residues in the HEAT repeats. As summarized in Fig. 8A, the positions of the prolines in importin-β1 are not well conserved at identical positions in distant species (Fig. 8A and Fig. S8, indicated by red boxes). However, judging from the human A-helix regions in the sequence alignment (Fig. S8, indicated by gray highlights), many prolines were found in potential A-helix regions of other species (Fig. S8, indicated by green boxes). When all of these potential A-helix prolines are taken into account, the importins of all species are predicted to contain a similar number of prolines in their A-helices, ranging from ∼12 to 15 (Fig. 8A). Although the degree of effect on molecular flexibility may be different for each proline residue, this suggests that the requirement for prolines in the structural maintenance of karyopherins follows a 'generous rule', in which their presence, but not exact position, is crucial.

It is intriguing that HEAT-rich proteins (such as PPP2R1A and CAND1) that do not belong to the karyopherin family also contain multiple proline residues in the A-helix (Fig. 8B). These proteins have been demonstrated to pass though the NPC and function as transport mediators (Fagotto et al., 1998; Koike et al., 2004; Wiechens and Fagotto, 2001; Yoshimura et al., 2014), suggesting that proline-containing HEAT repeats are involved in nuclear transport. Conversely, a number of HEAT repeats that do not contain proline in the A-helix (cohesion etc.) were found in the structural database. Although the consensus function of HEAT repeats is not understood fully (Yoshimura and Hirano, 2016), the fact that the bacterial protein YibA contains HEAT-like repetitive helices with multiple prolines in its outer α-helices (PDB: 1oyz) implies that the ancestral type of HEAT repeats might have contained proline residues in the A-helix. During evolution, some HEAT-repeat-containing proteins kept those prolines and started to become involved in nuclear transport. Other proteins might have lost their prolines and became involved in other cellular functions, such as mitotic chromosome segregation.

In addition to HEAT-repeat-containing proteins, proteins containing several amphiphilic helical motifs are able to pass through the nuclear pore spontaneously, including armadillo (ARM) repeats and spectrin repeats (Fagotto et al., 1998; Koike et al., 2004; Kumeta et al., 2010). Structural analyses of the typical ARM-containing proteins importin-α (PDB: 1ial) and β-catenin (PDB: 2bct) revealed the similar localization of multiple prolines in their outer helix (Fig. 8B). The total number of prolines in the outer helix is 8 and 10 for importin-α and β-catenin, respectively, which may be sufficient to maintain molecular flexibility and reversibility in a hydrophobic environment. Considering the nature of the NPC barrier, it is tempting to suggest that the proline-based strategy evolved a long time ago to achieve efficient nuclear transport.

The presence of proline residues in an α-helix has been regarded as problematic because of their ability to break its structure, and indeed there are several reports of proline mutations as a pathogenic mechanism (Yang et al., 1997). Here, we have reported the first example of the positive effect of proline residues in α-helices in the maintenance of a flexible molecular structure. It is interesting to note that prolines in protein molecules, which restrict polypeptide flexibility by possessing fixed ϕ and ψ angles, lead to the local destabilization of an α-helical structure, and finally contribute to the overall flexible molecular conformation of karyopherins (Fig. 8C). Thus, proline does not always serve as a 'breaker' of α-helical proteins, but rather behaves as a 'protector' of flexible molecular structure in some situations. Further studies focusing on the relations between molecular flexibility and functionality will

Journal of Cell Science (2018) 131, jcs206326. doi:10.1242/jcs.206326

**A**

| | same position | same helix | different helix | total |
|---|---|---|---|---|
| *Arabidopsis thaliana* | 6 | 3 | 3 | 12 |
| *Marchantia polymorpha* | 7 | 2 | 3 | 12 |
| *Chlamydomonas reinhardtii* | 9 | 2 | 4 | 15 |
| *Caenorhabditis elegans* | 8 | 2 | 3 | 13 |
| *Drosophila melanogaster* | 9 | 5 | 3 | 17 |
| *Danio rerio* | 15 | 0 | 0 | 15 |
| *Homo sapiens* | 15 | - | - | 15 |
| *Saccharomyces cerevisiae* | 5 | 3 | 4 | 12 |
| *Plasmodium falciparum* | 3 | 3 | 3 | 9 |
| *Trypanosoma brucei* | 5 | 7 | 2 | 14 |

**B**

| | # of repeats | # of proline residues: outer helix | inner helix | loop |
|---|---|---|---|---|
| HEAT repeat | | | | |
| importin β1 (mouse) | 19 | 15 | 1 | 21 |
| importin β1 (human) | 19 | 15 | 1 | 21 |
| importin β (S. Cerevisiae) | 19 | 11 | 1 | 22 |
| exportin 1 (human) | 19 | 11 | 0 | 29 |
| exportin 1 (S. Cerevisiae) | 19 | 18 | 2 | 23 |
| transportin (human) | 19 | 24 | 0 | 26 |
| PPP2R1A (human) | 15 | 14 | 1 | 11 |
| CAND1 (human) | 28 | 26 | 1 | 27 |
| ARM repeat | | | | |
| importin α (mouse) | 10 | 8 | 2 | 11 |
| β-catenin (human) | 12 | 10 | 2 | 6 |

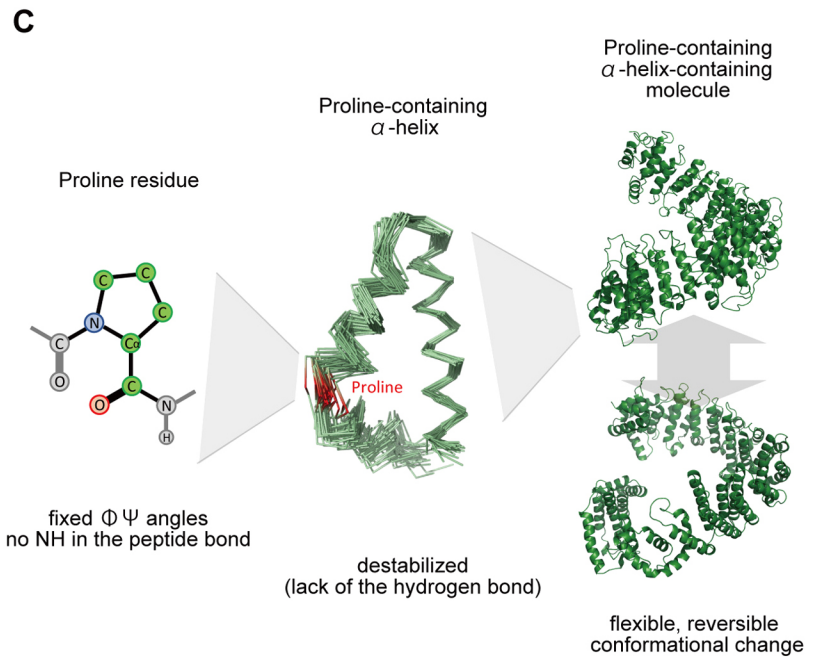


**Fig. 8. Evolutionary conservation and conceptual model of the maintenance of molecular flexibility for multiple proline-containing α-helix-containing molecules.** (A) Conservation of 15 prolines found in the A-helices of human importin-β1 was analyzed among nine eukaryotic species. Accession IDs for the sequences used are: Q9FJD4 (*Arabidopsis thaliana*), Mapoly0016s0170.1 (*Marchantia polymorpha*), A8HQU3 (*Chlamydomonas reinhardtii*), Q9BIB8 (*Caenorhabditis elegans*), O18388 (*Drosophila melanogaster*), A0A0R4IMZ8 (*Danio rerio*), Q14974 (*Homo sapiens*), Q06142 (*Saccharomyces cerevisiae*), Q8IAY9 (*Plasmodium falciparum*), and Q38BV5 (*Trypanosoma brucei*). The phylogenetic tree is shown on the left. Identical: prolines found at the same position as the human gene; similar: prolines not identical but found in the A-helix region of human importin-β1; total: total number of predicted prolines in the A-helix. The entire alignment is presented in Fig. S8. (B) Proline distribution of non-karyopherin HEAT proteins and ARM proteins. Secondary structure is determined based on the structural information registered in PDB: 1ukl (importin-β1, mouse), 1qgk (importin-β1, human), 3nd2 (importin-β, *S. cerevisiae*), 3g8b (exportin-1, human), 3vyc (exportin-1, *S. cerevisiae*), 2qmr (transportin, human), 2nyl (PPP2R1A, human), 1u6g (CAND1, human), 1ial (importin-α, mouse) and 2bct (β-catenin, human). (C) Proline is known to restrict the flexibility of a polypeptide chain due to its fixed ϕ and ψ angles. As a result of this property, proline is known as a breaker of α-helices by introducing a characteristic kink in the structure. The lack of a hydrogen at the nitrogen atom also results in destabilization of the helix. Although this mechanism is often known as a genetic cause of disease, it functions beneficially for a group of proteins enriched in α-helices. Multiple prolines in the α-helices work cooperatively to ensure a flexible conformational change of the entire molecule. In the case of importin-β, prolines play an essential role in its adaptive conformational change in a hydrophobic environment, and thus, ensure the proper function of the molecule as a nuclear transport mediator.

uncover the cellular strategy used to orchestrate the proper function of molecules working in a variety of different subcellular environments.

## MATERIALS AND METHODS

### DNA constructs

The plasmid encoding GST-HA-tagged mouse importin-β was described previously (Otsuka et al., 2008). A series of importin-β mutation fragments were amplified by overlap extension PCR from GST-HA-tagged mouse importin-β (ΔPro-I, ΔPro-II, ΔPro-III, ΔPro-IV and ΔPro-all) and cloned into the pGEX-2T vector (GE Healthcare). The importin-β genes were excised and cloned into pEGFP-C1 vector (Clontech-Takara) for EGFP fusion expression. cDNA fragments encoding full-length human Nup54, FG-rich regions of rat Nup62 (amino acid residues 1–178), human Nup153 (amino acid residues 896–1475), and the IBB of rat importin-α (amino acid residues 1–69) were amplified by PCR from full-length cDNA and cloned into the pGEX6P-2 vector (GE Healthcare). cDNAs encoding NLS of SV40 large T antigen (MPPKKKRKVED) and human histone H3 were cloned into the pmCherry–C1 and pmPlum–C1 vector (Clontech).

### Protein expression, purification and gel filtration

A series of GST-fused wild-type and mutant importin-β proteins were expressed in *Escherichia coli* strain BL21 codon Plus (Agilent Technologies) and protein expression was induced by adding IPTG (0.5 mM at 18°C for 6 h). Finally, the proteins were dialyzed with 100 mM $KPO_4$ after the GST tag was cleaved by biotinylated thrombin (Novagen). GST-importin-α IBB expression was induced by 0.5 mM IPTG at 18°C for 3 h and dialyzed with transport buffer consisting of 20 mM HEPES-KOH (pH 7.3), 110 mM $CH_3COOK$, 2 mM $(CH_3COO)_2Mg$, 5 mM $CH_3COONa$, 0.5 mM EGTA and 1 mM DTT after purification. GST-Nups were expressed in the same way and immobilized on glutathione Sepharose (GE Healthcare) for the binding assay. For the gel filtration assay, purified importin-β (wild-type and ΔPro-all, ∼10 µg) was subjected to gel filtration chromatography (Superdex 200; GE Healthcare) in 50 mM HEPES-KOH (pH 7.4), 100 mM NaCl, and 1 mM β-mercaptoethanol. The elution profiles were recorded and the molecular masses were estimated by the elution pattern of the markers.

### CD spectra

The CD spectra of purified proteins were measured using a JHL850 (Nihon-bunko) with a 0.1 cm cuvette at 20°C. Proteins were dissolved in 50 mM $KPO_4$ (pH 7.4).

### bis-ANS binding assay

The fluorescent measurements of bis-ANS (4,4′-dianilino-1,1′-binaphthyl-5,5′-disulfonic acid, dipotassium salt; Sigma-Aldrich) were performed with ARVO (Perkin Elmer) using emission and excitation wavelengths of 405 and 460 nm, respectively. Importin-β (final concentration, 0.5 µM) and bis-ANS (0.1–100 µM) were incubated in 50 µl transport buffer for 15 min at room temperature.

### Time-lapse imaging and kinetic analysis of GFP-labeled proteins

All cellular assays were performed using HeLa cells. For live cell observation, HeLa cells co-transfected with EGFP–importin-β and mPlum–Histone-H3 were observed in time-lapse under fluorescence microscopy (FV1200; Olympus) equipped with a stage-top heating

chamber (Tokai Hit). For the nuclear transport assay, HeLa cells were washed with transport buffer, incubated with 0.05% digitonin at 0°C for 15 min, washed twice with transport buffer, and incubated at 37°C for 15 min. Purified GFP-fused proteins (1–5 µM) were added, and nuclear accumulation was observed in time-lapse under fluorescence microscopy (PASCAL 5; Zeiss). To check the integrity of the nuclear envelope, 10 µg/ml Alexa Fluor 568-labeled IgG was added to the sample. All analyses were performed by MetaMorph software (Molecular Imaging). Curve fitting and other kinetic analyses of the obtained data were performed using Origin software (LightStone).

### Molecular dynamics simulation

Molecular dynamics simulations were conducted as described previously (Yoshimura et al., 2014), with the Amber11 package and an ff99SB force field. A GPU version of the particle mesh Ewald method was used with an NVIDIA Tesla M2090. The time step was set to 2 fs. Temperature was maintained at 310 K using Langevin dynamics with a collision frequency of 1.0 $ps^{-1}$; pressure was kept at 1 atm with a relaxation time of 2.0 ps. Bonds involving hydrogens were constrained with the SHAKE algorithm, and the long-range interaction cut-off was set to 10.0 Å. Before starting the production runs, the system underwent 100–500 ps equilibration with weak position restraint on the protein. The obtained datasets are available from the corresponding author upon reasonable request.

### FRAP analysis and curve fitting

EGFP-fused importin-β (wild-type and mutants) was expressed in HeLa cells. FRAP analysis was performed with a laser scanning confocal microscope (FV-1200; Olympus) equipped with a 37°C heating stage and 5% $CO_2$ supply. During the time-lapse observations (1.7 s/frame), the nucleus was irradiated by a bleach laser (488 nm) for 1 s. After bleaching, the time-lapse observations were continued for 100 s. Fluorescent recovery for the nuclear membrane region and nucleoplasm was quantified and analyzed statistically. Curve fitting was performed using data analysis software (Origin; LightStone) with the following fitting functions: for the nuclear envelope, $y=I_{final}\times(1-(k_{on}/(k_{on}+k_{off}))\times\exp(-k_{off}\times x))$; for the nucleoplasm: $y=\exp(-x\times k_{out})\times Y_0+(k_{in}/k_{out})\times(1-\exp(-x\times k_{out}))$.

### Urea-denaturation assay

Purified wild-type and mutant importin-β were mixed with various concentrations of urea (0–9 M) (final concentration of importin-β was 0.1 mg/ml in 50 mM $KPO_4$, pH 7.4) and/or TFE (0–50%). The fluorescence spectrum of the protein solution was measured with an excitation wavelength of 320 nm by a fluorescence spectrometer (FP8300; JASCO). The center wavelength of the emission peak was plotted against the concentration of urea. The *m*-value and folding free energy ($\Delta G_0$) were obtained as described previously (Eftink, 1994).

#### Acknowledgements

We thank S. Iwasaka, K. Ogawa, Y. Takashima, S. Asai and R. Watanabe for technical assistance.

#### Competing interests

The authors declare no competing or financial interests.

#### Author contributions

Conceptualization: M.K., S.H.Y.; Methodology: M.K., H.A.K., S.H.Y.; Formal analysis: M.K., H.A.K., W.Z., S.S., S.H.Y.; Investigation: M.K., H.A.K., W.Z., S.S., S.H.Y.; Writing - original draft: M.K., S.H.Y.; Writing - review & editing: M.K., H.A.K., W.Z., S.S., S.H.Y.; Project administration: S.H.Y.; Funding acquisition: M.K., S.H.Y.

#### Funding

This work was supported by a Grant-in-Aid for Scientific Research on Priority Areas (to S.H.Y.) from the Japanese Ministry of Education, Culture, Sports, Science and Technology, by Grants-in-Aid for Basic Research (B) (to S.H.Y.), for a Young Scientist (A) (to S.H.Y.) and for a Young Scientist (B) (to M.K.) from the Japan Society for the Promotion of Science, by the Funding Program for Next Generation World-leading Researchers (to S.H.Y.), and by the Cross-Disciplinary Research Promotion Project (to M.K.) from iCeMS, Kyoto University.

#### Supplementary information

Supplementary information available online at
http://jcs.biologists.org/lookup/doi/10.1242/jcs.206326.supplemental

#### References

**Barlow, D. J. and Thornton, J. M.** (1988). Helix geometry in proteins. *J. Mol. Biol.* **201**, 601-619.

**Bayliss, R., Ribbeck, K., Akin, D., Kent, H. M., Feldherr, C. M., Görlich, D. and Stewart, M.** (1999). Interaction between NTF2 and xFxFG-containing nucleoporins is required to mediate nuclear import of RanGDP. *J. Mol. Biol.* **293**, 579-593.

**Bayliss, R., Littlewood, T. and Stewart, M.** (2000). Structural basis for the interaction between FxFG nucleoporin repeats and importin-beta in nuclear trafficking. *Cell* **102**, 99-108.

**Bayliss, R., Littlewood, T., Strawn, L. A., Wente, S. R. and Stewart, M.** (2002). GLFG and FxFG nucleoporins bind to overlapping sites on importin-beta. *J. Biol. Chem.* **277**, 50597-50606.

**Bednenko, J., Cingolani, G. and Gerace, L.** (2003). Importin beta contains a COOH-terminal nucleoporin binding region important for nuclear transport. *J. Cell Biol.* **162**, 391-401.

**Ben-Efraim, I. and Gerace, L.** (2001). Gradient of increasing affinity of importin beta for nucleoporins along the pathway of nuclear import. *J. Cell Biol.* **152**, 411-417.

**Chi, N. C. and Adam, S. A.** (1997). Functional domains in nuclear import factor p97 for binding the nuclear localization sequence receptor and the nuclear pore. *Mol. Biol. Cell* **8**, 945-956.

**Chook, Y. M. and Blobel, G.** (1999). Structure of the nuclear transport complex karyopherin-beta2-Ran x GppNHp. *Nature* **399**, 230-237.

**Chook, Y. M. and Blobel, G.** (2001). Karyopherins and nuclear import. *Curr. Opin. Struct. Biol.* **11**, 703-715.

**Ciciarello, M., Mangiacasale, R., Thibier, C., Guarguaglini, G., Marchetti, E., Di Fiore, B. and Lavia, P.** (2004). Importin beta is transported to spindle poles during mitosis and regulates Ran-dependent spindle assembly factors in mammalian cells. *J. Cell Sci.* **117**, 6511-6522.

**Cingolani, G., Petosa, C., Weis, K. and Müller, C. W.** (1999). Structure of importin-beta bound to the IBB domain of importin-alpha. *Nature* **399**, 221-229.

**Cingolani, G., Lashuel, H. A., Gerace, L. and Müller, C. W.** (2000). Nuclear import factors importin alpha and importin beta undergo mutually induced conformational changes upon association. *FEBS Lett.* **484**, 291-298.

**Conti, E., Müller, C. W. and Stewart, M.** (2006). Karyopherin flexibility in nucleocytoplasmic transport. *Curr. Opin. Struct. Biol.* **16**, 237-244.

**Cronshaw, J. M., Krutchinsky, A. N., Zhang, W., Chait, B. T. and Matunis, M. J.** (2002). Proteomic analysis of the mammalian nuclear pore complex. *J. Cell Biol.* **158**, 915-927.

**Eftink, M. R.** (1994). The use of fluorescence methods to monitor unfolding transitions in proteins. *Biophys. J.* **66**, 482-501.

**Fagotto, F., Glück, U. and Gumbiner, B. M.** (1998). Nuclear localization signal-independent and importin/karyopherin-independent nuclear import of beta-catenin. *Curr. Biol.* **8**, 181-190.

**Forwood, J. K., Lange, A., Zachariae, U., Marfori, M., Preast, C., Grubmüller, H., Stewart, M., Corbett, A. H. and Kobe, B.** (2010). Quantitative structural analysis of importin-beta flexibility: paradigm for solenoid protein structures. *Structure* **18**, 1171-1183.

**Frey, S. and Gorlich, D.** (2006). FG-rich repeats of nuclear pore proteins form a three-dimensional meshwork with hydrogel-like properties. *Science* **314**, 815-817.

**Görlich, D. and Kutay, U.** (1999). Transport between the cell nucleus and the cytoplasm. *Annu. Rev. Cell Dev. Biol.* **15**, 607-660.

**Harel, A. and Forbes, D. J.** (2004). Importin beta: conducting a much larger cellular symphony. *Mol. Cell* **16**, 319-330.

**Harel, A., Chan, R. C., Lachish-Zalait, A., Zimmerman, E., Elbaum, M. and Forbes, D. J.** (2003). Importin beta negatively regulates nuclear membrane fusion and nuclear pore complex assembly. *Mol. Biol. Cell* **14**, 4387-4396.

**Henderson, R., Baldwin, J. M., Ceska, T. A., Zemlin, F., Beckmann, E. and Downing, K. H.** (1990). Model for the structure of bacteriorhodopsin based on high-resolution electron cryo-microscopy. *J. Mol. Biol.* **213**, 899-929.

**Hetzer, M., Gruss, O. J. and Mattaj, I. W.** (2002). The Ran GTPase as a marker of chromosome position in spindle formation and nuclear envelope assembly. *Nat. Cell Biol.* **4**, E177-E184.

**Koike, M., Kose, S., Furuta, M., Taniguchi, N., Yokoya, F., Yoneda, Y. and Imamoto, N.** (2004). beta-Catenin shows an overlapping sequence requirement but distinct molecular interactions for its bidirectional passage through nuclear pores. *J. Biol. Chem.* **279**, 34038-34047.

**Konishi, H. A., Asai, S., Watanabe, T. M. and Yoshimura, S. H.** (2017). In vivo analysis of protein crowding within the nuclear pore complex in interphase and mitosis. *Sci. Rep.* **7**, 5709.

**Kose, S., Imamoto, N., Tachibana, T., Shimamoto, T. and Yoneda, Y.** (1997). Ran-unassisted nuclear migration of a 97-kD component of nuclear pore-targeting complex. *J. Cell Biol.* **139**, 841-849.

**Kumeta, M., Yoshimura, S. H., Harata, M. and Takeyasu, K.** (2010). Molecular mechanisms underlying nucleocytoplasmic shuttling of actinin-4. *J. Cell Sci.* **123**, 1020-1030.

**Kumeta, M., Yamaguchi, H., Yoshimura, S. H. and Takeyasu, K.** (2012). Karyopherin-independent spontaneous transport of amphiphilic proteins through the nuclear pore. *J. Cell Sci.* **125**, 4979-4984.

**Lee, S. J., Imamoto, N., Sakai, H., Nakagawa, A., Kose, S., Koike, M., Yamamoto, M., Kumasaka, T., Yoneda, Y. and Tsukihara, T.** (2000). The adoption of a twisted structure of importin-beta is essential for the protein-protein interaction required for nuclear transport. *J. Mol. Biol.* **302**, 251-264.

**Liu, S. M. and Stewart, M.** (2005). Structural basis for the high-affinity binding of nucleoporin Nup1p to the Saccharomyces cerevisiae importin-beta homologue, Kap95p. *J. Mol. Biol.* **349**, 515-525.

**Lott, K., Bhardwaj, A., Mitrousis, G., Pante, N. and Cingolani, G.** (2010). The importin beta binding domain modulates the avidity of importin beta for the nuclear pore complex. *J. Biol. Chem.* **285**, 13769-13780.

**Luecke, H., Schobert, B., Richter, H.-T., Cartailler, J.-P. and Lanyi, J. K.** (1999). Structure of bacteriorhodopsin at 1.55 A resolution. *J. Mol. Biol.* **291**, 899-911.

**Lummis, S. C. R., Beene, D. L., Lee, L. W., Lester, H. A., Broadhurst, R. W. and Dougherty, D. A.** (2005). Cis-trans isomerization at a proline opens the pore of a neurotransmitter-gated ion channel. *Nature* **438**, 248-252.

**Mackay, D. R., Elgort, S. W. and Ullman, K. S.** (2009). The nucleoporin Nup153 has separable roles in both early mitotic progression and the resolution of mitosis. *Mol. Biol. Cell* **20**, 1652-1660.

**Mitsuoka, K., Hirai, T., Murata, K., Miyazawa, A., Kidera, A., Kimura, Y. and Fujiyoshi, Y.** (1999). The structure of bacteriorhodopsin at 3.0 A resolution based on electron crystallography: implication of the charge distribution. *J. Mol. Biol.* **286**, 861-882.

**Mohr, D., Frey, S., Fischer, T., Guttler, T. and Görlich, D.** (2009). Characterisation of the passive permeability barrier of nuclear pore complexes. *EMBO J.* **28**, 2541-2553.

**Mosammaparast, N. and Pemberton, L. F.** (2004). Karyopherins: from nuclear-transport mediators to nuclear-function regulators. *Trends Cell Biol.* **14**, 547-556.

**Muhlhäusser, P. and Kutay, U.** (2007). An in vitro nuclear disassembly system reveals a role for the RanGTPase system and microtubule-dependent steps in nuclear envelope breakdown. *J. Cell Biol.* **178**, 595-610.

**Nachury, M. V., Maresca, T. J., Salmon, W. C., Waterman-Storer, C. M., Heald, R. and Weis, K.** (2001). Importin beta is a mitotic target of the small GTPase Ran in spindle assembly. *Cell* **104**, 95-106.

**O'Neil, K. T. and DeGrado, W. F.** (1990). A thermodynamic scale for the helix-forming tendencies of the commonly occurring amino acids. *Science* **250**, 646-651.

**O'Reilly, A. J., Dacks, J. B. and Field, M. C.** (2011). Evolution of the karyopherin-beta family of nucleocytoplasmic transport factors; ancient origins and continued specialization. *PLoS ONE* **6**, e19308.

**Otsuka, S., Iwasaka, S., Yoneda, Y., Takeyasu, K. and Yoshimura, S. H.** (2008). Individual binding pockets of importin-beta for FG-nucleoporins have different binding properties and different sensitivities to RanGTP. *Proc. Natl. Acad. Sci. USA* **105**, 16101-16106.

**Pemberton, L. F. and Paschal, B. M.** (2005). Mechanisms of receptor-mediated nuclear import and nuclear export. *Traffic* **6**, 187-198.

**Piela, L., Nemethy, G. and Scheraga, H. A.** (1987). Proline-induced constraints in alpha-helices. *Biopolymers* **26**, 1587-1600.

**Rout, M. P., Aitchison, J. D., Suprapto, A., Hjertaas, K., Zhao, Y. and Chait, B. T.** (2000). The yeast nuclear pore complex: composition, architecture, and transport mechanism. *J. Cell Biol.* **148**, 635-651.

**Sprague, B. L., Muller, F., Pego, R. L., Bungay, P. M., Stavreva, D. A. and McNally, J. G.** (2006). Analysis of binding at a single spatially localized cluster of binding sites by fluorescence recovery after photobleaching. *Biophys. J.* **91**, 1169-1191.

**Stewart, M.** (2007). Molecular mechanism of the nuclear protein import cycle. *Nat. Rev. Mol. Cell Biol.* **8**, 195-208.

**Wiechens, N. and Fagotto, F.** (2001). CRM1- and Ran-independent nuclear export of beta-catenin. *Curr. Biol.* **11**, 18-28.

**Wigley, W. C., Corboy, M. J., Cutler, T. D., Thibodeau, P. H., Oldan, J., Lee, M. G., Rizo, J., Hunt, J. F. and Thomas, P. J.** (2002). A protein sequence that can encode native structure by disfavoring alternate conformations. *Nat. Struct. Biol.* **9**, 381-388.

**Xu, D., Farmer, A. and Chook, Y. M.** (2010). Recognition of nuclear targeting signals by Karyopherin-beta proteins. *Curr. Opin. Struct. Biol.* **20**, 782-790.

**Yang, J.-M., Yoneda, K., Morita, E., Imamura, S., Nam, K., Lee, E.-S. and Steinert, P. M.** (1997). An alanine to proline mutation in the 1A rod domain of the keratin 10 chain in epidermolytic hyperkeratosis. *J. Invest. Dermatol.* **109**, 692-694.

**Yoshimura, S. H. and Hirano, T.** (2016). HEAT repeats - versatile arrays of amphiphilic helices working in crowded environments? *J. Cell Sci.* **129**, 3963-3970.

**Yoshimura, S. H., Kumeta, M. and Takeyasu, K.** (2014). Structural mechanism of nuclear transport mediated by importin beta and flexible amphiphilic proteins. *Structure* **22**, 1699-1710.

## Supplementary Information

**Fig. S1. Western blot and subcellular localization of EGFP-fused mutants expressed in HeLa cells.**

(A) HeLa cells expressing EGFP-fused importin β (wild-type, *Δ*Pro-I, II, III, IV, and all) were harvested 24 hours post-transfection, and subjected to the anti-EGFP Western blot. Lysates correspond to 0.6-25 × $10^4$ cells were loaded for each lanes. Single bands around 120 kDa were detected, which correspond to the full-length EGFP-fused importin β.

(B) HeLa cells expressing EGFP-importin β (wild-type, *Δ*Pro-I, II, III, IV, and all) were observed under confocal laser scanning microscope with the same acquisition setting. Typical images were shown.

(C) From the microscopic images, the averaged signal intensities of the whole cells were statistically compared. Although the mutants tended to express less, there were no significant differences among their expression levels (P > 0.05).

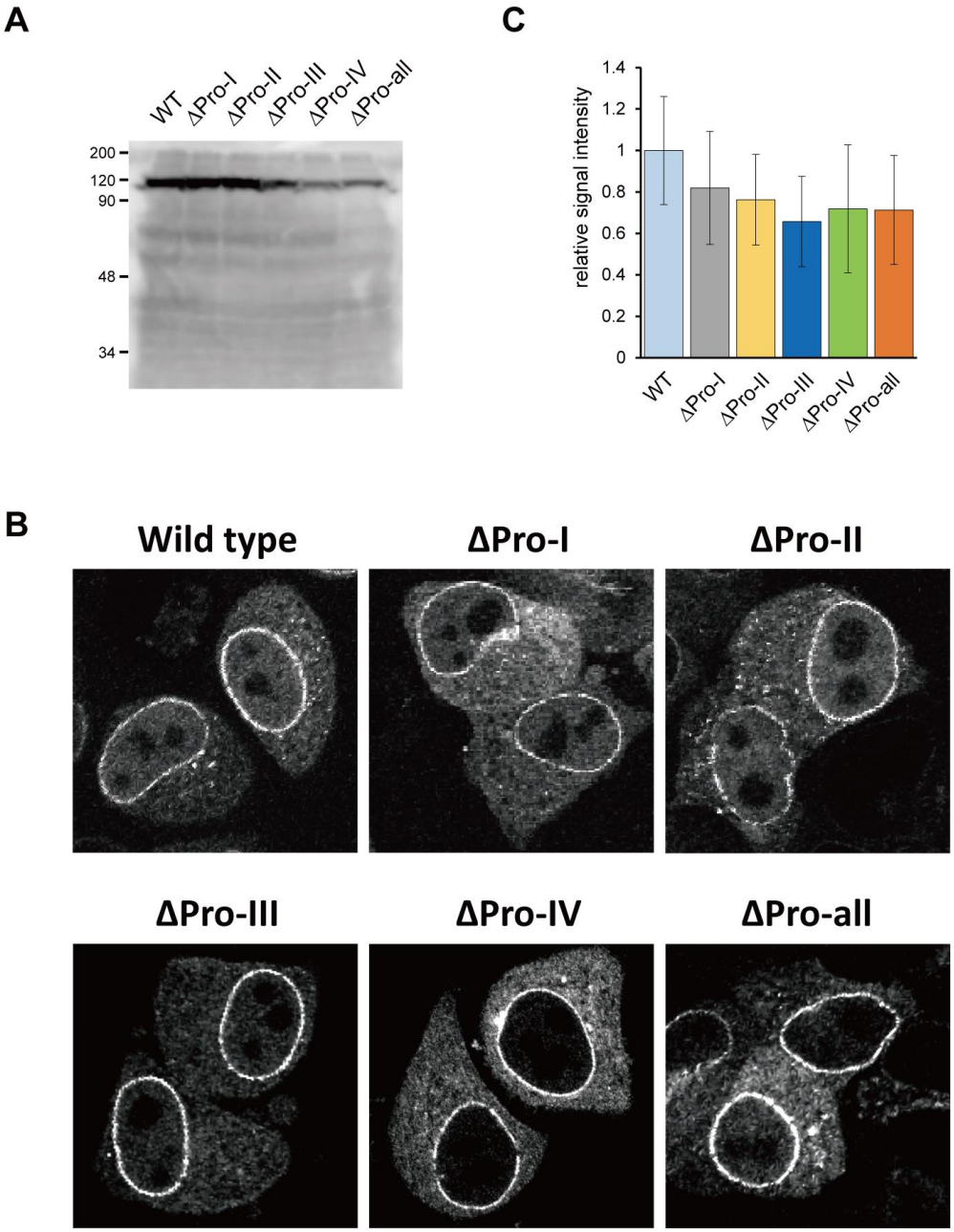

**Fig. S2. Mitotic defects of cells expressing EGFP-importin β ⊿Pro-all.**
Mitotic dynamics of a HeLa cell expressing importin β ⊿Pro-all was followed by florescent microscope. Images for EGFP-importin β ⊿Pro-all (green) and mPlum-Histone H3 (magenta) taken every 10 min were presented until the cell showed abnormal bleb structure (180-190 min).

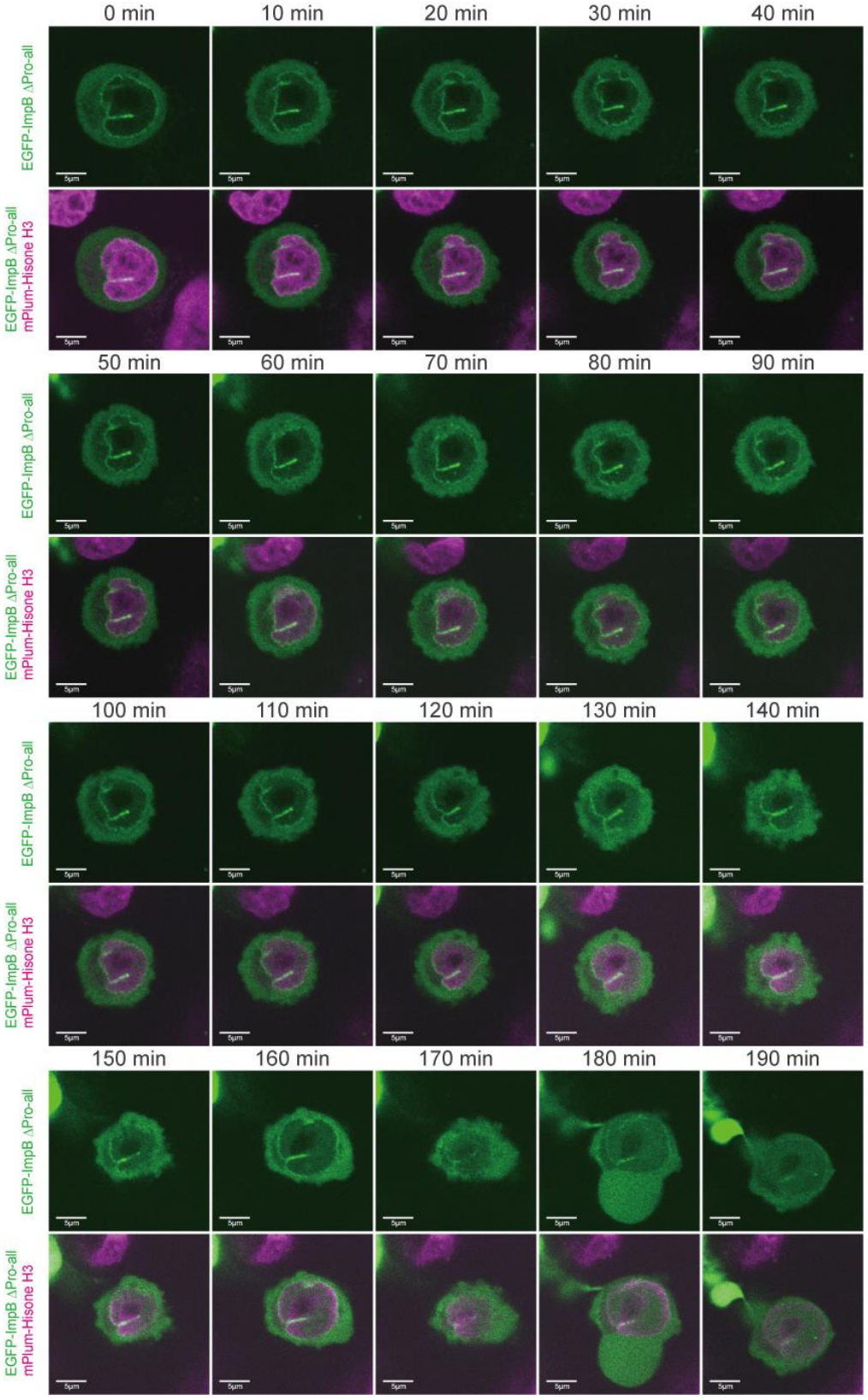

**Fig. S3. Curve fitting analyses for the FRAP results.**
(A) FRAP results presented in Fig. 3B (nuclear envelope) were used to obtain kinetic parameters ($I_{final}$ and $k_{on}$) by the curve fitting analyses. Actual measurement values are presented in black, and the fitted curves were shown in red, for wile-type and each mutants. The fitting function is described in the Materials and Methods.
(B) FRAP results presented in Fig. 3C (nucleoplasm) were used to obtain kinetic parameter ($k_{in}$) by the curve fitting analyses.

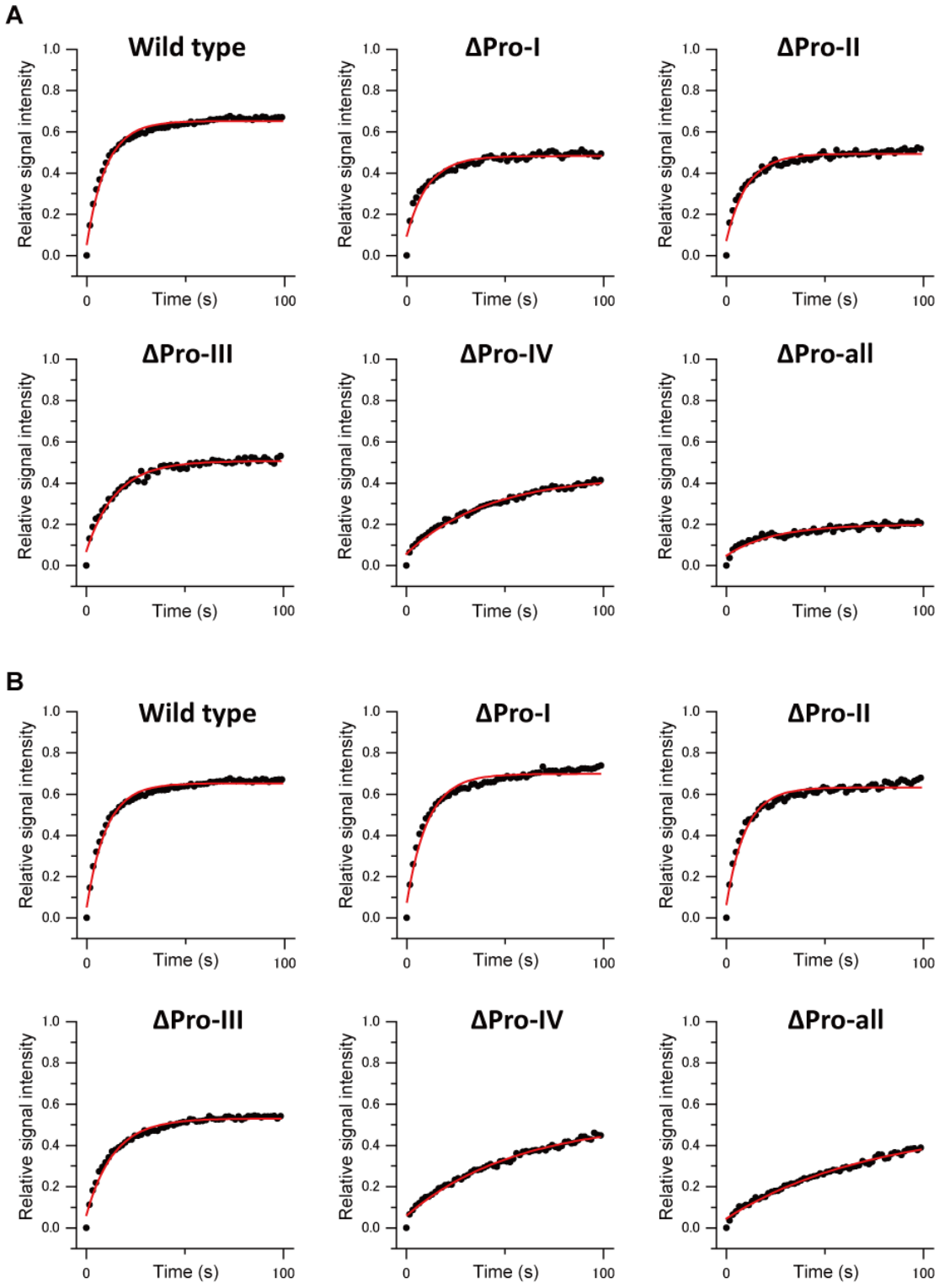

**Fig. S4. CD spectrum measurements of wild-type and mutant importin β.**
CD spectra of wild-type and mutant importin β in 50 mM $KPO_4$. Similar α-helix-rich spectra with two characteristic negative peaks were obtained for all proteins.

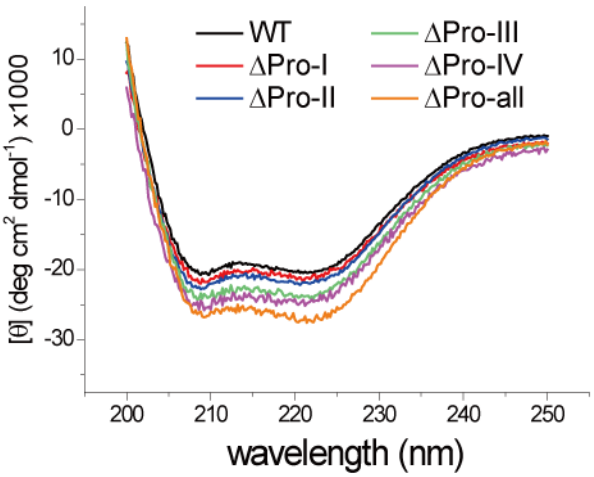

**Fig. S5. Tryptophan fluorescent spectra for wild-type importin β denatured under 0–9 M urea in water or in the presence of TFE.**

Tryptophan fluorescence was measured for wild-type importin β denatured in different concentrations of urea in water or in the presence of 5–20% TFE. The signal was measured in 0.5 nm pitches. Three independent measurements were performed and averaged spectra are shown.

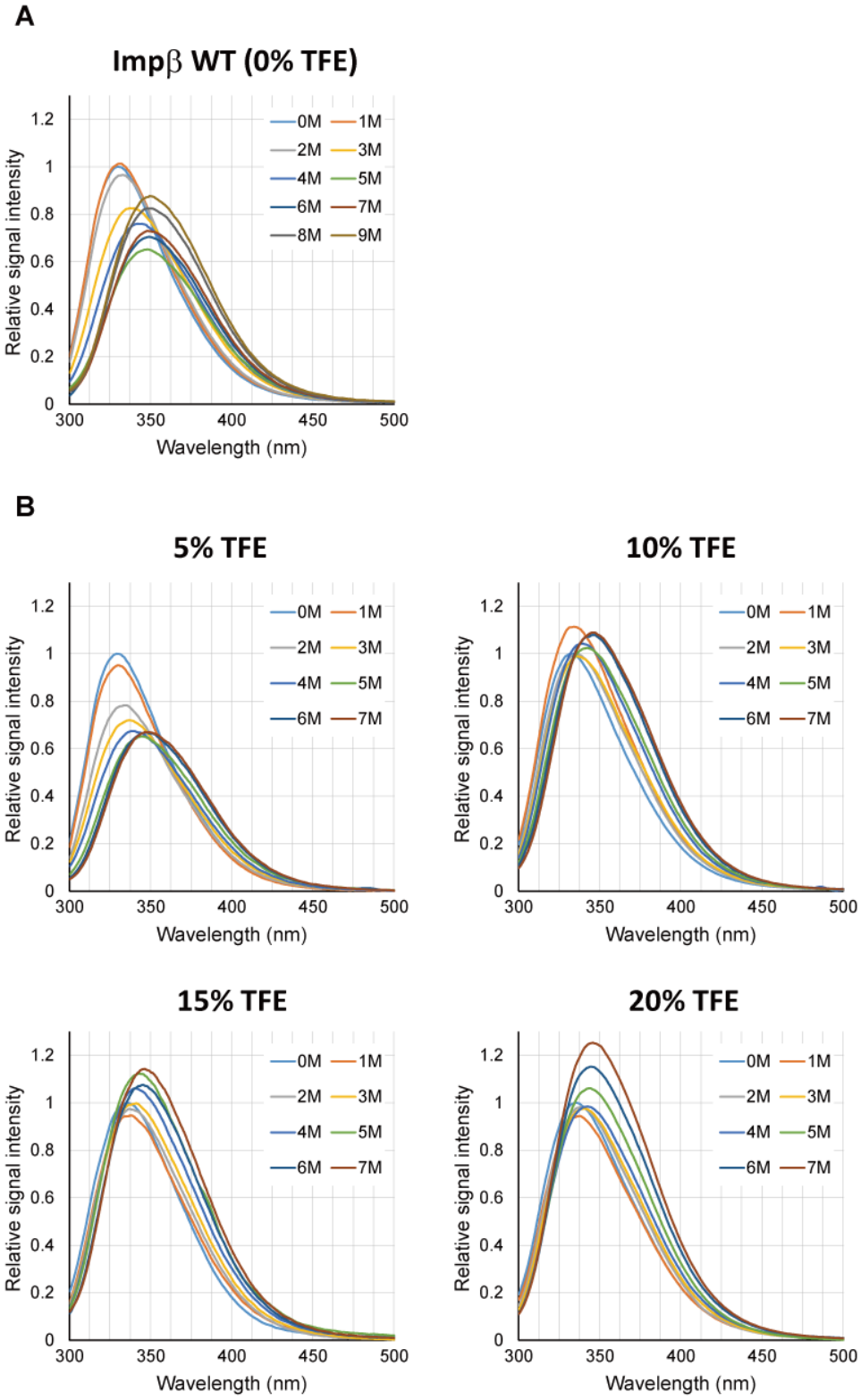

**Fig. S6. Tryptophan fluorescent spectra for wild-type and mutant importin β in the presence of 0–50% TFE.**

Tryptophan fluorescence was measured for wild-type and mutant importin β, as well as N-acetyl tryptophan, in the presence of 0–50% TFE (without urea). The signal was measured in 0.5 nm pitches. More than 4 independent measurements were performed and averaged spectra are shown. The apparent decrease in peak fluorescent intensity was the effect of TFE, as free N-acetyl tryptophan spectra also showed a similar decrease.

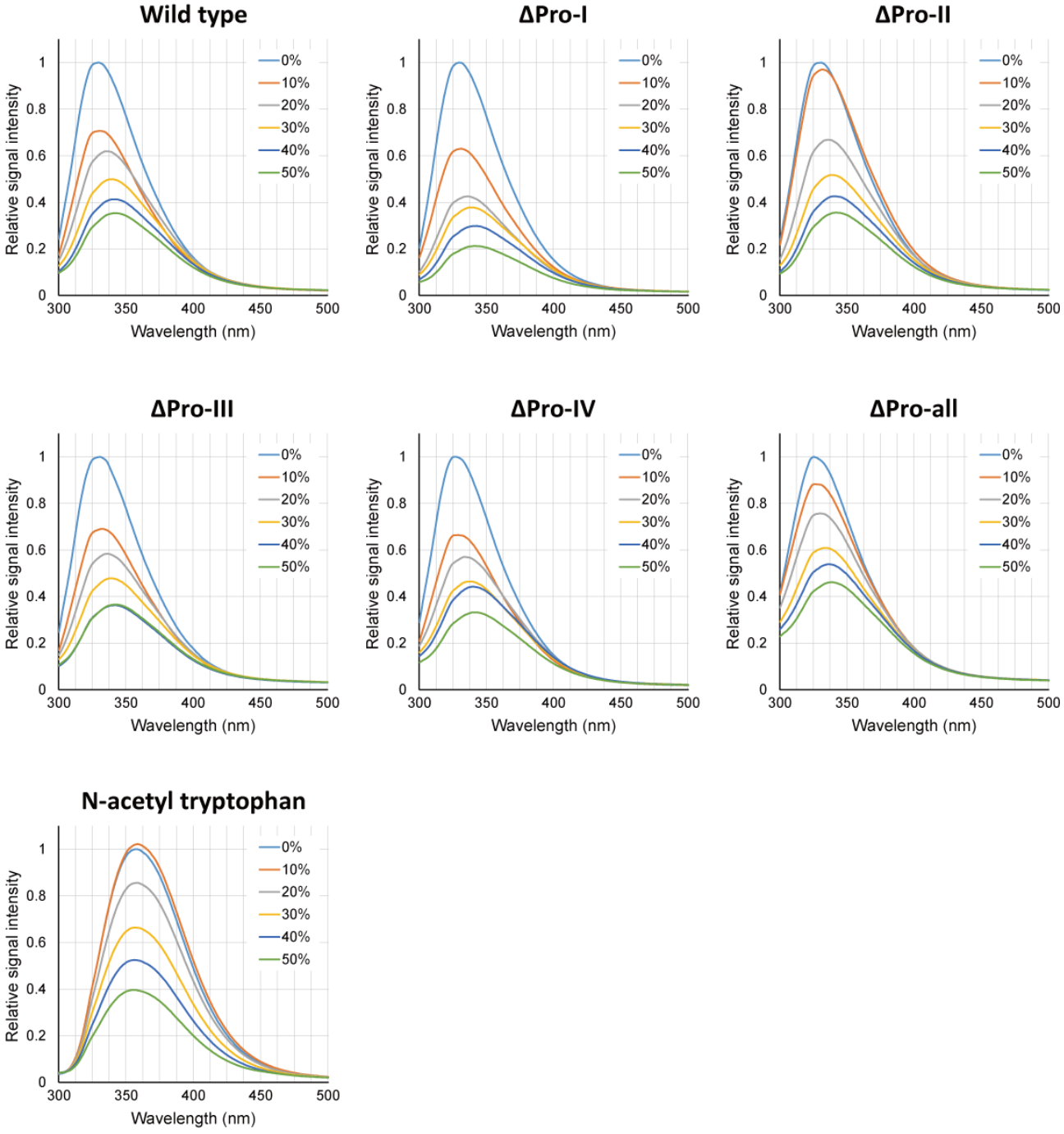

**Fig. S7. Status of each helix in different environments evaluated by molecular dynamics simulation.**

(A) Relative changes in the distance between adjacent HEAT motifs were estimated by analyzing the displacement of the center of each helix in the last 50 ns of molecular dynamics simulation.

(B) Relative changes in the length of the A-helices were measured in the last 50 ns of molecular dynamics simulation.

(C) Kink angle of helices around proline analyzed for wild-type and *Δ*Pro-all mutant importin β in water. There were no significant differences among them.

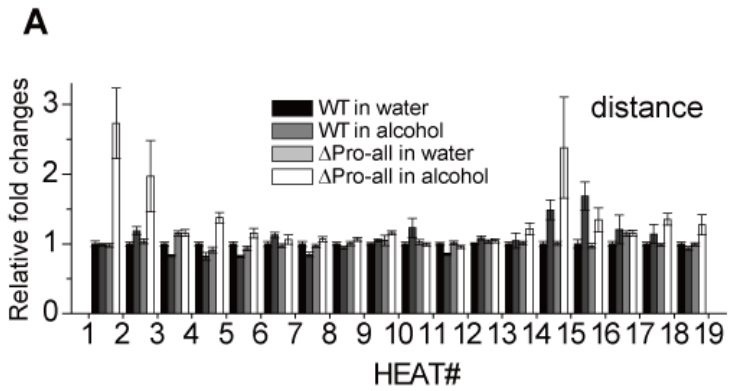


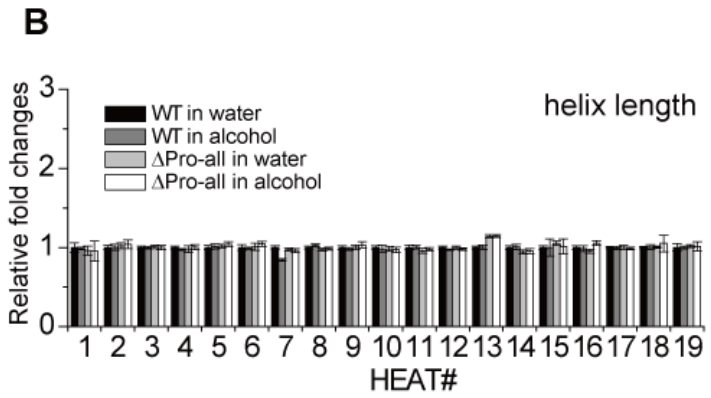


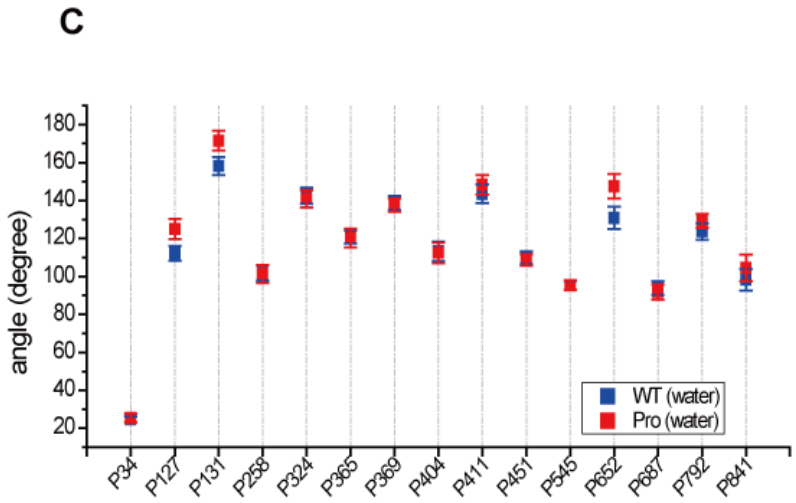

## Fig. S8. Alignment of importin β1 from 10 eukaryotic species.

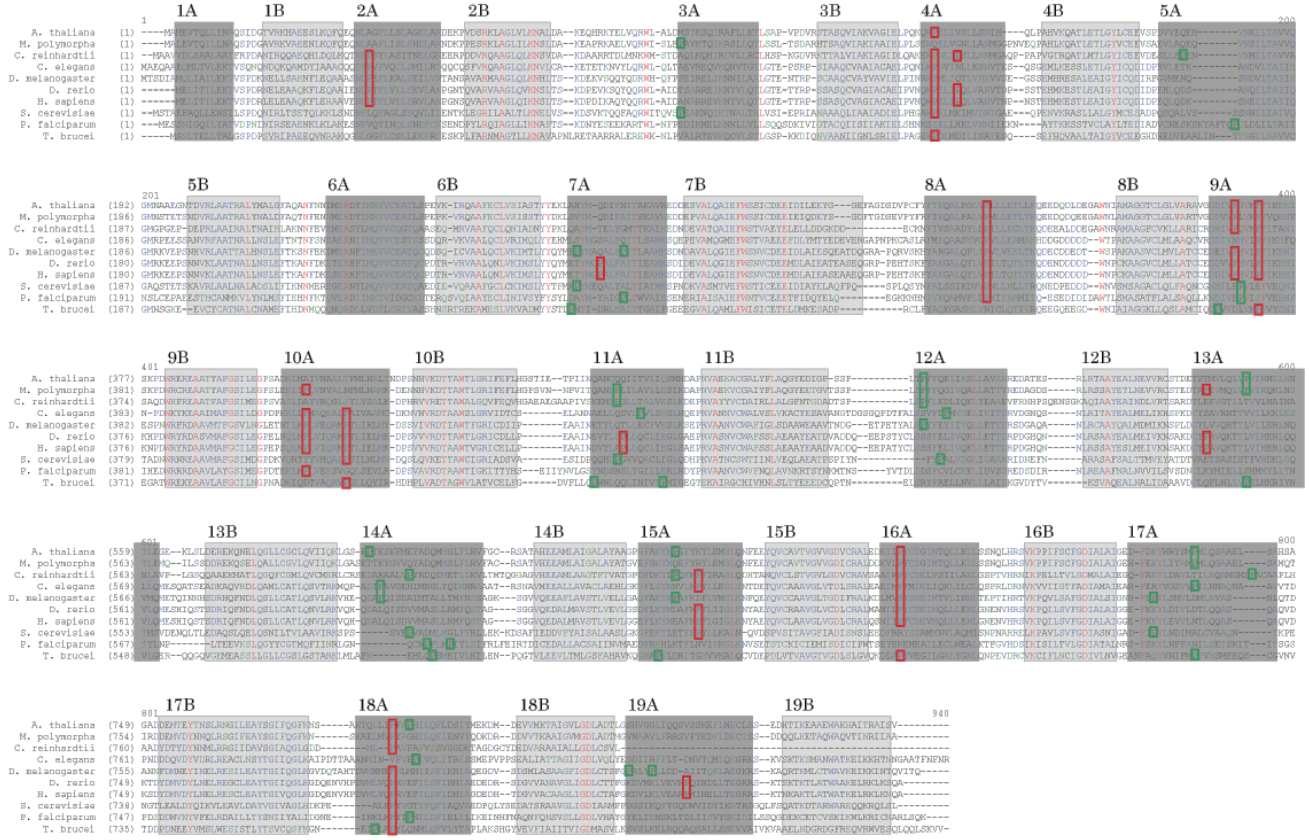


Red: identical amino acids, Blue: conservative, Green: weakly similar

Darl gray highlights: human A-helix regions, Light gray highlights: human B-helix regions

□: A-helix proline identical with human (same position), □: potential A-helix proline found in human A-helix region

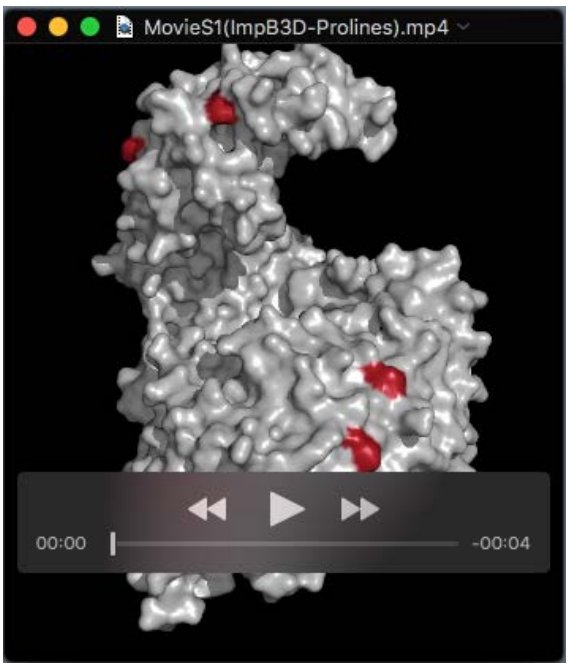


**Movie S1. Proline locations indicated in 3D structure of importin β.**
A 3D rotation movie of importin β (PDB: 1ukl) molecule shown in a surface representation. 15 proline residues in A-helix are indicated in red.


**Movie S2. Time-lapse movie of mitotic HeLa cells expressing EGFP-fused wild-type importin β.**
Mitotic HeLa cells expressing EGFP-importin β and mPlum-histone H3 were observed under a confocal laser scanning microscope. Images were taken every 2 min. Breakdown and reformation of the nuclear membrane were observed.


**Movie S3. Time-lapse movie of mitotic HeLa cells expressing EGFP-fused ⊿Pro-all importin β.** Mitotic HeLa cells expressing EGFP-fused ⊿Pro-all mutant importin β and mPlum-histone H3 were observed under a confocal laser scanning microscope. Images were taken every 2 min. The nuclear membrane did not breakdown throughout the observation period (50 min in total).